High Catalytic Rates for Hydrogen Production Using Nickel Electrocatalysts with Seven-Membered Cyclic Diphosphine Ligands Containing One Pendant Amine

ARTICLE *in* JOURNAL OF THE AMERICAN CHEMICAL SOCIETY · FEBRUARY 2013

Impact Factor: 12.11 · DOI: 10.1021/ja400181a · Source: PubMed

8 AUTHORS, INCLUDING:

Ming-Hsun Ho
Pacific Northwest National Laboratory
22 PUBLICATIONS **325** CITATIONS
SEE PROFILE

Stefan Wiese
Air Liquide
9 PUBLICATIONS **242** CITATIONS
SEE PROFILE

Mary Lou Lindstrom
University of Nevada, Reno
3 PUBLICATIONS **59** CITATIONS
SEE PROFILE

Simone Raugei
Pacific Northwest National Laboratory
96 PUBLICATIONS **1,743** CITATIONS
SEE PROFILE

JACS
JOURNAL OF THE AMERICAN CHEMICAL SOCIETY
Article
pubs.acs.org/JACS

High Catalytic Rates for Hydrogen Production Using Nickel Electrocatalysts with Seven-Membered Cyclic Diphosphine Ligands Containing One Pendant Amine

Michael P. Stewart, Ming-Hsun Ho, Stefan Wiese, Mary Lou Lindstrom, Colleen E. Thogerson, Simone Raugei, R. Morris Bullock, and Monte L. Helm*

Center for Molecular Electrocatalysis, Physical Sciences Division, Pacific Northwest National Laboratory, P.O. Box 999, K2-57, Richland, Washington 99352, United States

Supporting Information

ABSTRACT: A series of Ni-based electrocatalysts, $[Ni(7P^{Ph}_2N^{C6H4X})_2](BF_4)_2$, featuring seven-membered cyclic diphosphine ligands incorporating a single amine base, 1-*para*-X-phenyl-3,6-triphenyl-1-aza-3,6-diphosphacycloheptane ($7P^{Ph}_2N^{C6H4X}$, where X = OMe, Me, Br, Cl, or CF_3), have been synthesized and characterized. X-ray diffraction studies have established that the $[Ni(7P^{Ph}_2N^{C6H4X})_2]^{2+}$ complexes have a square planar geometry, with bonds to four phosphorus atoms of the two bidentate diphosphine ligands. Each of the complexes is an efficient electrocatalyst for hydrogen production at the potential of the Ni(II/I) couple, with turnover frequencies ranging from 2400 to 27 000 s^{-1} with $[(DMF)H]^+$ in acetonitrile. Addition of water (up to 1.0 M) accelerates the catalysis, giving turnover frequencies ranging from 4100 to 96 000 s^{-1}. Computational studies carried out on the $[Ni(7P^{Ph}_2N^{C6H4X})_2]^{2+}$ family indicate the catalytic rates reach a maximum when the electron-donating character of X results in the pK_a of the Ni(I) protonated pendant amine matching that of the acid used for proton delivery. Additionally, the fast catalytic rates for hydrogen production by the $[Ni(7P^{Ph}_2N^{C6H4X})_2]^{2+}$ family relative to the analogous $[Ni(P^{Ph}_2N^{C6H4X}_2)_2]^{2+}$ family are attributed to preferred formation of endo protonated isomers with respect to the metal center in the former, which is essential to attain suitable proximity to the reduced metal center to generate H_2. The results of this work highlight the importance of precise pK_a matching with the acid for proton delivery to obtain optimal rates of catalysis.

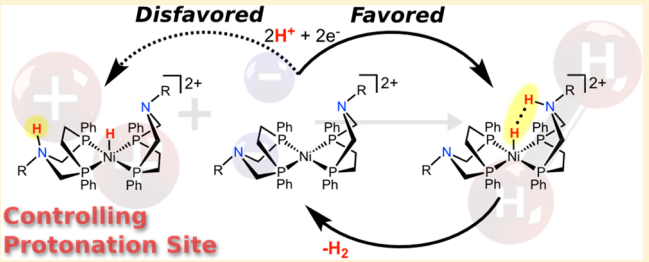

INTRODUCTION

The expanded use of energy from intermittent renewable energy sources such as solar and wind will require the ability to efficiently convert electricity to chemical energy for storage as fuels. Efficient catalysts are necessary for both the production and the utilization of hydrogen. Platinum and the hydrogenase enzymes are excellent catalysts for both production and oxidation of hydrogen. Platinum, however, is a precious metal with high cost and low abundance.[1] Hydrogenase enzymes, while remarkably efficient catalysts in nature,[2−4] are expensive to obtain in large amounts and difficult to adapt to large-scale commercial applications. These considerations have spawned efforts to design molecular catalysts that employ more abundant metals, such as nickel,[5] cobalt,[6−14] iron,[15−28] or molybdenum,[29−31] as electrocatalysts for the production and oxidation of hydrogen.[32,33]

Efforts in our laboratory have focused on developing first-row metal complexes (Ni,[5,34,35] Co,[10,14] Fe,[36] and Mn[37]) that contain an amine base in the second coordination sphere, adjacent to a vacant coordination site or a hydride ligand on the metal center. These mononuclear complexes, in which the base facilitates the heterolytic cleavage/formation of the H−H bond and functions as a proton relay,[38] mimic an important structural feature proposed for the active site of [FeFe]-hydrogenase enzymes, the presence of an azadithiolate ligand in the dinuclear active site, shown in structure **1**.[3,4,23] Nickel and cobalt diphosphine complexes that incorporate a positioned base in the ligand have been found to be active electrocatalysts for hydrogen production in acidic acetonitrile solutions, and the Fe complexes with similar ligands exhibit evidence for heterolytic cleavage and oxidation of H_2.[5,35,36]

Using a series of $[Ni(P^R_2N^{R'}_2)_2]^{2+}$ catalysts, where P_2N_2 stands for a 1,3-R′-3,7-R derivative of 1,5-diaza-3,7-diphosphacyclooctane, we have previously examined how the basicity of the proton relay in cooperation with the size and electronic characteristics of the substituent at the phosphorus atoms influence the turnover frequencies for H_2 production.[39−42] Under optimized conditions, $[Ni(P^{Ph}_2N^{C6H4Br}_2)_2]^{2+}$ (structure **2**, X = Br), containing electron-withdrawing bromo substituents on the aniline rings of the ligand and phenyl groups on the phosphorus atoms, catalyzed the formation of H_2 with turnover

Received: January 7, 2013
Published: February 5, 2013

dx.doi.org/10.1021/ja400181a | J. Am. Chem. Soc. 2013, 135, 6033−6046

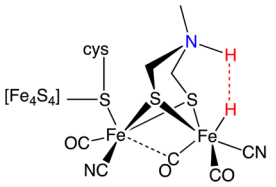

1

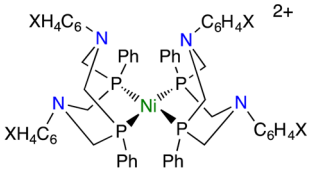

2

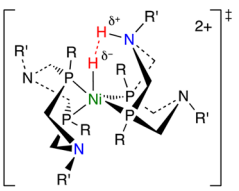

3

frequencies as high as 1040 s^{-1} and an overpotential of approximately 290 mV.[39]

The positioned amines in the second coordination sphere play important roles in the catalytic activity of these complexes. Our experimental and theoretical mechanistic studies of $[Ni(P^{R}_2N^{R'}_2)_2]^{2+}$ catalysts suggest that the transition state for heterolytic H−H bond formation and cleavage has structure **3**.[38,43−45] Further studies on the reduction and protonation of closely related analogues of **2** have shown that intermediates formed during the catalytic cycle potentially include isomeric Ni(0) complexes in which an amine in each ligand is protonated.[34,46−49] The kinetically formed doubly protonated Ni(0) species has both protons in exo positions relative to the nickel center, "pinched" between the two pendant amines with N−H···N bonding. Isomerization to form endo protonated species that would be active in the catalytic cycle has been shown to involve intermolecular deprotonation by a base followed by reprotonation at an endo position.[48] These studies led us to propose that only a fraction of the doubly protonated Ni(0) intermediates formed during hydrogen production are in the catalytically active form and that higher catalytic rates might be achieved if the stabilized exo protonated structures could be avoided.[39,47,48] We now present a study of related nickel bis(diphosphine) catalysts that contain ligands that are structurally modified, but which still retain features that allow access to similar transition state structures.[50] In this Article, we report turnover frequencies up to 96 000 s^{-1} for electrocatalytic hydrogen production with overpotentials ranging from 550 to 640 mV using a modified nickel catalyst containing two seven-membered cyclic diphosphine ligands $7P^{Ph}_2N^{C6H4X}$ (where $7P^{Ph}_2N^{C6H4X}$ is 1-*para*-X-phenyl-3,6-triphenyl-1-aza-3,6-diphosphacycloheptane and X = OMe, Me, Br, Cl, or CF_3). Factors that may contribute to the rates are discussed, including the effects of changing from eight-membered to seven-membered cyclic ligands and the impact of reducing the number of amine bases in the ligand backbones.

RESULTS

Synthesis and Characterization of Ligands and Complexes. The synthesis of 1-*para*-X-phenyl-3,6-triphenyl-1-aza-3,6-diphosphacycloheptane ligands ($7P^{Ph}_2N^{C6H4X}$, where X = OMe (**4-OMe**), Me (**4-Me**), Br (**4-Br**), Cl (**4-Cl**), and CF_3 (**4-CF_3**)) was accomplished through the addition of 1 equiv of a *p*-substituted aniline to 1,2-bis(hydroxymethylphenylphosphino)ethane in CH_3CN and refluxing for 12 h, as previously reported for **4-H** (X = H)[51] and shown in eq 1. The cyclic ligands containing a seven-membered ring are formed as approximately 1:1 mixtures of racemic and meso isomers as indicated by $^{31}P\{^1H\}$ NMR spectra of the crude reaction mixtures. Recrystallization results in pure ligand, although as a mixture of the *meso*- and *rac*-isomers, which show one singlet each in their $^{31}P\{^1H\}$ NMR spectra. ^1H and $^{31}P\{^1H\}$ NMR spectral data for each ligand are provided in the Experimental Section, and these spectra are consistent with the formulations of these ligands.

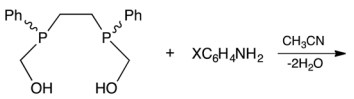

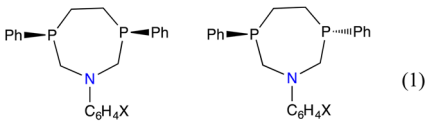

meso-7-$P^{Ph}_2N^{C6H4X}$ *rac*-7-$P^{Ph}_2N^{C6H4X}$

(1)

4-OMe	X = OMe	**4-Br**	X = Br
4-Me	X = Me	**4-Cl**	X = Cl
4-H	X = H	**4-CF_3**	X = CF_3

The synthesis of the nickel complex of **4-H** was reported previously, and a similar route is followed here.[50] The addition of 2 equiv of **4-OMe**, **4-Me**, **4-Br**, **4-Cl**, or **4-CF_3** to an CH_3CN solution of $[Ni(CH_3CN)_6](BF_4)_2$ results in the formation of $[Ni(7P^{Ph}_2N^{C6H4X})_2](BF_4)_2$ (where X = OMe, Me, Br, Cl, or CF_3, **5-OMe**, **5-Me**, **5-Br**, **5-Cl**, or **5-CF_3**), as determined by $^{31}P\{^1H\}$ NMR spectroscopy and shown in eq 2. In addition to the homoleptic, monometallic complexes, the formation of oligomeric metal complexes is suggested by broad resonances in the $^{31}P\{^1H\}$ NMR spectra. Because a mixture of *meso*- and *rac*-isomers of **4** was used, the *rac*-isomers may function as bridging ligands between Ni(II) centers to form oligomeric byproducts. The desired monometallic complexes are isolated as orange crystalline products in yields ranging from 26% to 54% by concentration of the reaction mixture and crystallization by addition of CH_2Cl_2 followed by Et_2O. Each of the products has been fully characterized by NMR spectroscopy, elemental analyses, and single-crystal X-ray crystallography.

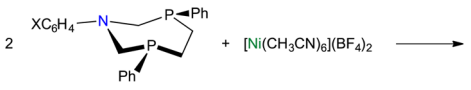

$7P^{Ph}_2N^{C6H4X}$

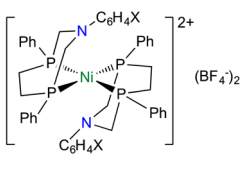

$[Ni(7P^{Ph}_2N^{C6H4X})_2]^{2+}$

(2)

5-OMe	X = OMe	**5-Br**	X = Br
5-Me	X = Me	**5-Cl**	X = Cl
5-H	X = H	**5-CF_3**	X = CF_3

dx.doi.org/10.1021/ja400181a | J. Am. Chem. Soc. 2013, 135, 6033−6046

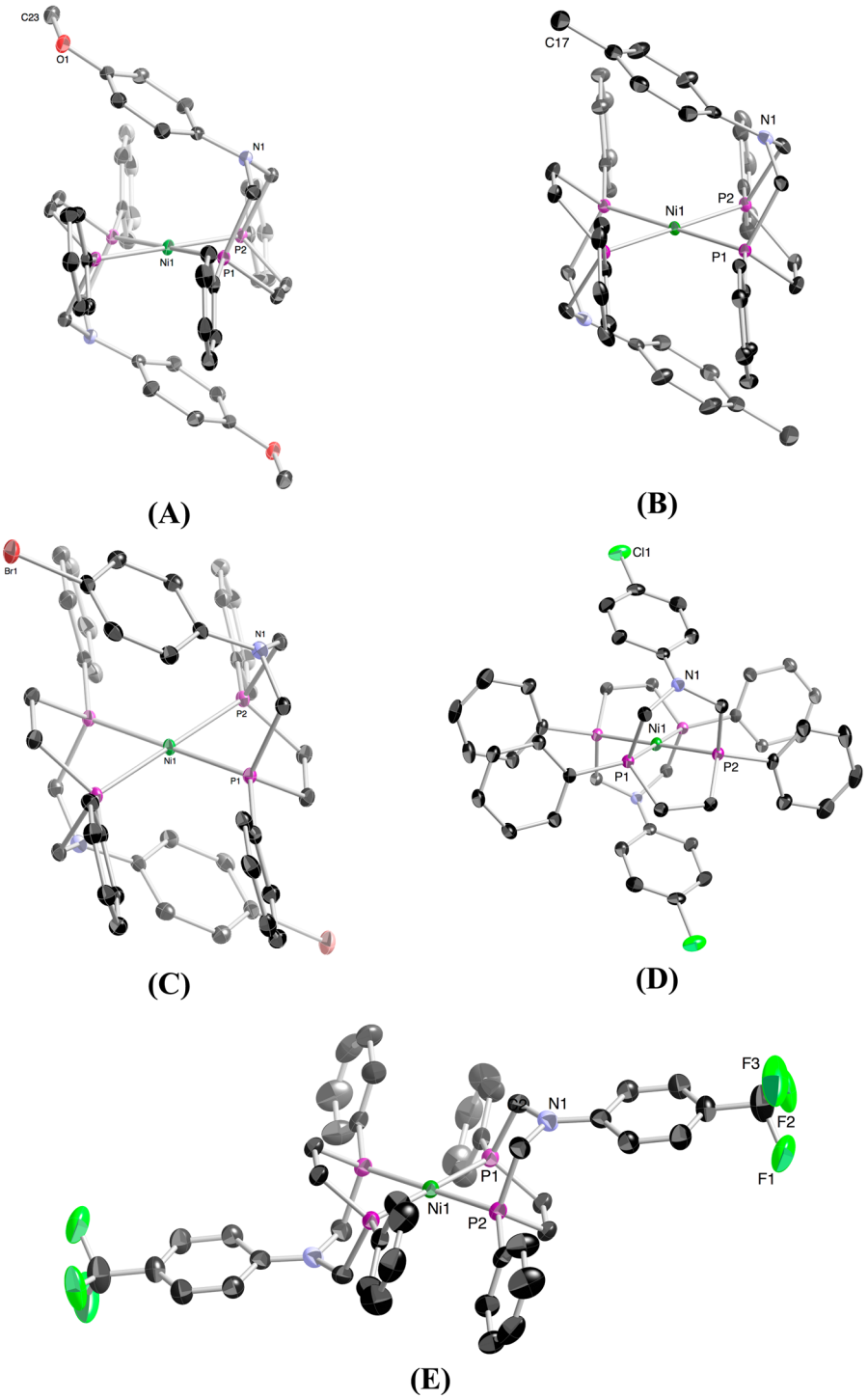

Figure 1. X-ray crystal structure of (A) $[Ni(7P^{Ph}{}_2N^{C6H4OMe})_2](BF_4)_2{\cdot}2CH_3CN$, **5-OMe**, (B) $[Ni(7P^{Ph}{}_2N^{C6H4Me})_2](BF_4)_2{\cdot}2CH_3CN$, **5-Me**, (C) $[Ni(7P^{Ph}{}_2N^{C6H4Br})_2](BF_4)_2{\cdot}2CH_3CN$, **5-Br**, (D) $[Ni(7P^{Ph}{}_2N^{C6H4Cl})_2](BF_4)_2{\cdot}2CH_3CN$, **5-Cl**, and (E) $[Ni(7P^{Ph}{}_2N^{C6H4CF3})_2](BF_4)_2{\cdot}2CH_3CN$, **5-CF$_3$**. The BF_4^- counterions, CH_3CN solvent molecules, and H atoms have been omitted for clarity. Thermal ellipsoids are all shown at the 50% probability level.

X-ray quality crystals of **5-OMe**, **5-Me**, **5-Br**, **5-Cl**, and **5-CF$_3$** were grown by slow diffusion of Et_2O into saturated CH_3CN or CH_2Cl_2 solutions of the complexes. The Ni(II) complexes **5-OMe**, **5-Me**, **5-Br**, and **5-Cl** complexes crystallize with two noncoordinating CH_3CN molecules per unit cell, and no close contacts are observed between the BF_4^- anions and any of these $[Ni(7P^{Ph}{}_2N^{C6H4X})_2]^{2+}$ cations. Complex **5-CF$_3$** crystallizes with no solvents and shows the BF_4^- anions interacting with the metal center, resulting in a pseudo-octahedral structure around the Ni center, with Ni···F distances of 3.02 Å (not shown in Figure 1E). A drawing of each cation is shown in Figure 1. The structures confirm that the ligands coordinate as diphosphine chelates to give a distorted square planar geometry with all four Ni–P bond distances nearly equal, ranging from 2.20 to 2.23 Å. The P–Ni–P bite angle for each of the diphosphine ligands spans a narrow range from 79.7° to 80.1°.

dx.doi.org/10.1021/ja400181a | J. Am. Chem. Soc. 2013, 135, 6033–6046

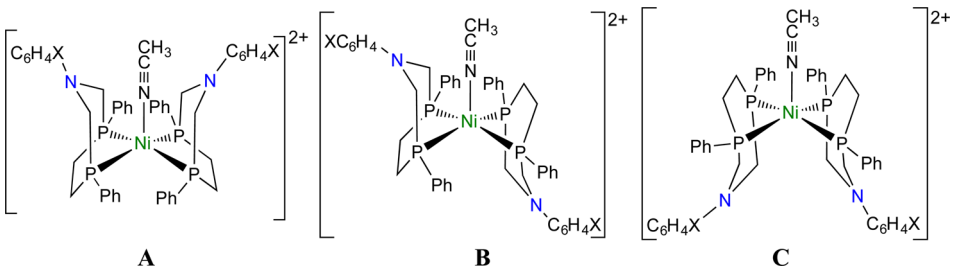

Figure 2. Proposed isomers of **5** in CH_3CN.

This angle is smaller than the 82−84° typically observed for the P−Ni−P bite angle in $[Ni(P^R{}_2N^{R'}{}_2)_2]^{2+}$ complexes,[39,40] which form two six-membered chelate rings upon binding to the metal. In contrast, for the $[Ni(7P^{Ph}{}_2N^{C6H4X})_2]^{2+}$ complexes, one five-membered and one six-membered ring formed upon chelation of the ligand. The smaller bite angle of $7P^{Ph}{}_2N^{C6H4X}$ as compared to the $P^{Ph}{}_2N^{R'}{}_2$ ligands results in a decrease in the steric interactions between the phenyl substituents on adjacent phosphorus atoms of the two ligands[39] and a more planar structure than observed in the corresponding $[Ni(P^{Ph}{}_2N^{R'}{}_2)_2]^{2+}$ cations. For example, in $[Ni(P^{Ph}{}_2N^{C6H4Me}{}_2)_2]^{2+}$, the dihedral angle between the two planes defined by the Ni atom and the two phosphorus atoms of each diphosphine ligand is 24.16°,[39] whereas it is 0.0° for $[Ni(7P^{Ph}{}_2N^{C6H4Me})_2]^{2+}$, as in all of the $[Ni(7P^{Ph}{}_2N^{C6H4X})_2]^{2+}$ structures. Thus, the replacement of one six-membered chelate with a five-membered ring has significant structural consequences for these complexes. As shown in Figure 1, the two six-membered rings containing the pendant amines are trans to each other across the metal center, and, except for **5-CF$_3$**, adopt boat conformations. The chair conformations of the six-membered rings observed in **5-CF$_3$** likely result from the interaction of the BF_4^- anions with the metal center in the solid state. The nonbonding Ni···N distances are 3.17−3.23 Å for **5-OMe**, **5-Me**, **5-Br**, and **5-Cl**, where the six-membered ring is in the boat conformation, and 3.68 Å for **5-CF$_3$**, where the six-membered ring is in the chair conformation. Complete crystallographic information along with bond distances and angles for **5-OMe**, **5-Me**, **5-Br**, **5-Cl**, and **5-CF$_3$** are contained in the Supporting Information.

The $^{31}P\{^1H\}$ NMR spectra of **5-OMe**, **5-Me**, **5-Br**, **5-Cl**, and **5-CF$_3$** in CD_2Cl_2 consist of a single peak ranging from 44.6 ppm for **5-OMe** to 41.8 ppm for **5-CF$_3$**. The ^1H NMR spectra of **5-OMe**, **5-Me**, **5-Br**, **5-Cl**, and CF_3 in CD_2Cl_2 also show the expected number and intensity of peaks consistent with the four-coordinate X-ray structures. The $^{31}P\{^1H\}$ NMR spectra of **5-OMe**, **5-Me**, **5-Br**, **5-Cl**, and **5-CF$_3$** in acetonitrile-d_3, however, consist of two peaks, a broad singlet (ranging from 51.8 to 48.8 ppm) and a sharp singlet (ranging from 47.2 to 45.2 ppm). In acetonitrile it is believed that the compounds are five-coordinate species with an acetonitrile bound to the nickel center, as previously reported for **5-H**.[50] As shown in Figure 2, this results in the possibility of three distinct isomers. Low-temperature $^{31}P\{^1H\}$ and ^1H NMR data in acetonitrile-d_3 indicate isomers **A** and **C** are rapidly interconverting through the dissociation/association of acetonitrile, resulting in the broad downfield singlet observed at room temperature. Isomer **B** has two different ligand environments; however, dissociation/association of the acetonitrile results in a chemically equivalent complex and therefore the sharper upfield chemical shift.

Table 1. Selected Electrochemical Data for $[Ni(7P^{Ph}{}_2N^{C6H4X})_2]^{2+}$ Complexes in 0.10 M $[Bu_4N][PF_6]$/CH_3CN

complex	overlapping Ni(II/I, I/0) observed $E_{1/2}$[a,b] (V)	ΔE_p[c] (mV)
$[Ni(7P^{Ph}{}_2N^{C6H4OMe})_2]^{2+}$, **5-OMe**	−1.14	120
$[Ni(7P^{Ph}{}_2N^{C6H4Me})_2]^{2+}$, **5-Me**	−1.13	120
$[Ni(7P^{Ph}{}_2N^{Ph})_2]^{2+}$, **5-H**	−1.12	105
$[Ni(7P^{Ph}{}_2N^{C6H4Br})_2]^{2+}$, **5-Br**	−1.08	104
$[Ni(7P^{Ph}{}_2N^{C6H4Cl})_2]^{2+}$, **5-Cl**	−1.08	120
$[Ni(7P^{Ph}{}_2N^{C6H4CF3})_2]^{2+}$, **5-CF$_3$**	−1.05	82

[a]All potentials are referenced to the $Cp_2Fe^{+/0}$ couple at 0 V. [b]Calculated as the average of the potentials of the maximum cathodic and anodic current. [c]Peak-to-peak separation of cathodic and anodic waves at a scan rate of 0.1 V/s.

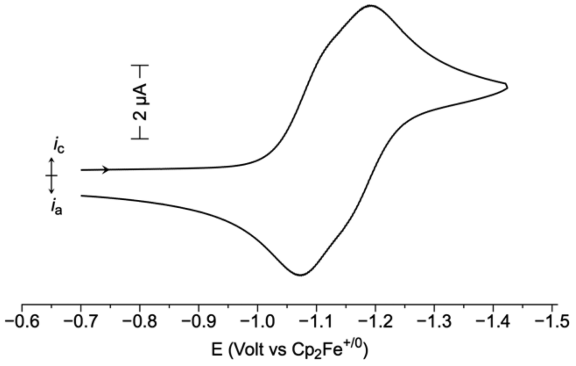

Figure 3. Cyclic voltammogram of 1.0 mM $[Ni(7P^{Ph}{}_2N^{C6H4OMe})_2]^{2+}$, **5-OMe**, in 0.10 M $[Bu_4N][PF_6]/CH_3CN$. Conditions: 1 mm glassy carbon working electrode; scan rate 0.1 V/s at 25 °C.

Electrochemical Studies. The cyclic voltammograms of **5-OMe**, **5-Me**, **5-Br**, **5-Cl**, and **5-CF$_3$** indicate two overlapping one-electron reversible redox couples, with observed $E_{1/2}$ values (reported as the average of the potentials of the maximum cathodic and anodic current) ranging from −1.05 to −1.14 V versus the ferrocenium/ferrocene ($Cp_2Fe^{+/0}$) couple, as summarized in Table 1 (e.g., **5-OMe**, Figure 3). A plot of the peak current (i_p) versus the square root of the scan rate shows a linear correlation in all cases, implying diffusion-controlled electrochemical events.[52] The difference in the potential of cathodic and anodic peak potentials (ΔE_p) at a scan rate of 0.1 V/s for these processes is measured to be 120−82 mV (Table 1), where the ΔE_p of $Cp_2Fe^{+/0}$ ranges from 68 to 71 mV. The observation that the ΔE_p values for the $[Ni(7P^{Ph}{}_2N^{C6H4X})_2]^{2+}$

dx.doi.org/10.1021/ja400181a | J. Am. Chem. Soc. 2013, 135, 6033−6046

family are neither 70 mV, as observed for the one-electron $Cp_2Fe^{+/0}$ couple, nor close to 30 mV, as predicted for a two-electron process, suggest that **5-OMe**, **5-Me**, **5-Br**, **5-Cl**, and **5-CF_3** undergo two, overlapping, one-electron processes as previously observed and simulated for **5-H** (the determination of i_p for the catalytic rate calculations is discussed below).[50] In the analogous $[Ni(P^{Ph}{}_2N^{C6H4X}{}_2)_2]^{2+}$ systems (e.g., **2**), an increase in basicity of the pendant amine results in a negative shift of the redox potential of the complex. The same trend is observed here, with **5-OMe** having the most negative redox potential at −1.14 V and **5-CF_3** having the most positive redox potential at −1.05 V.[39] The observed trend in redox potentials is also in accordance with that predicted by the "electrochemical ligand parameter" (E_L) series developed by Lever, which catalogs common substituents by their electron-donating/-withdrawing ability.[53,54]

Electrocatalytic Production of Hydrogen. When electrochemical measurements on **5-OMe**, **5-Me**, **5-Br**, **5-Cl**, and **5-CF_3** are carried out in the presence of acid, a large increase in the cathodic peak current is observed (e.g., **5-Br**, Figure 4).

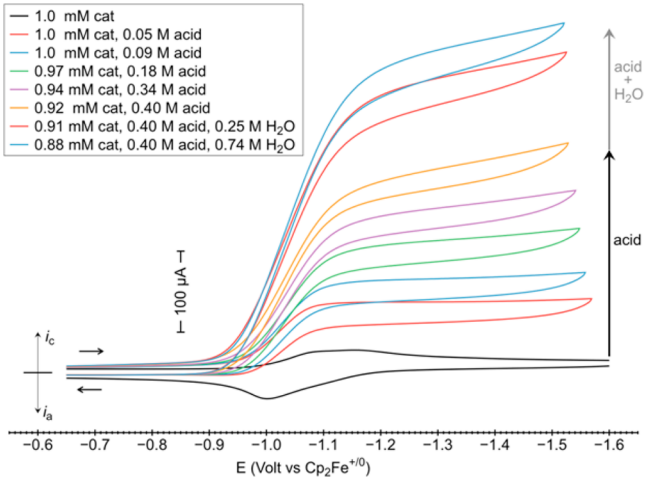

Figure 4. Cyclic voltammograms of $[Ni(7P^{Ph}{}_2N^{C6H4Br})_2]^{2+}$, **5-Br**, in 0.10 M $[Bu_4N][PF_6]/CH_3CN$ with subsequent additions of $[(DMF)H]^+$ and H_2O. Conditions: 1 mm glassy carbon working electrode; 25 °C; scan rate 10 V/s.

Protonated dimethylformamide triflate, $[(DMF)H]OTf$ (pK_a = 6.1 in MeCN), a crystalline solid,[55] was used as the acid.[56,57] Figure 5 shows that a plot of the catalytic current (i_{cat}) versus $[(DMF)H^+]^{1/2}$ gives a linear correlation, indicating the reaction is first-order with respect to acid concentration (i.e., eq 3, where n is the number of electrons involved in the catalytic reaction, F is Faraday's constant, A is the area of the electrode, D is the diffusion coefficient, k is the rate constant, and x is the order of the reaction with respect to acid).[58−61]

$$i_{cat} = nFA[cat]\sqrt{D(k[H^+]^x)} \quad (3)$$

The observed catalytic current (i_{cat}) in cyclic voltammograms recorded at slower scan rates (ca. <0.5 V/s) deviated from the plateau shape expected for catalytic waves by displaying a moderate scan rate dependence below scan rates of 1 V/s, as well as peak-shaped diffusion-controlled wave forms (e.g., **5-OMe**, Figure 6), as previously described for **5-H**.[50] These wave shapes have been attributed to significant depletion of acidic substrate at the electrode as expected for very fast catalysts. For each catalyst, detailed studies were conducted to determine the

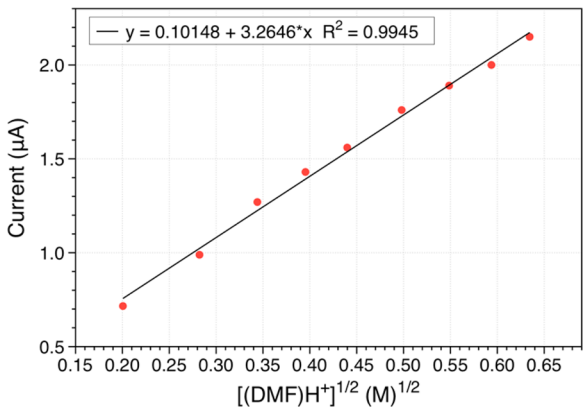

Figure 5. Plot of i_{cat} versus $[(DMF)H^+]^{1/2}$ for $[Ni(7P^{Ph}{}_2N^{C6H4Br})_2]^{2+}$, **5-Br**, measured in 0.10 M $[Bu_4N][PF_6]/CH_3CN$ with increasing concentrations of $[(DMF)H]^+$. Conditions: 1 mm glassy carbon working electrode; 25 °C; scan rate 10 V/s.

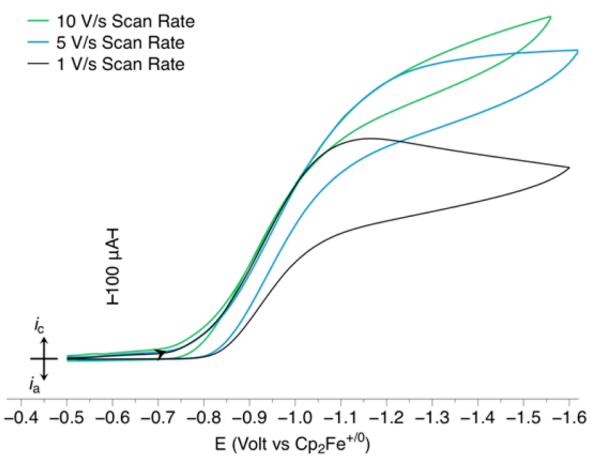

Figure 6. Cyclic voltammograms of 1.0 mM $[Ni(7P^{Ph}{}_2N^{C6H4OMe})_2]^{2+}$, **5-OMe**, in 0.10 M $[Bu_4N][PF_6]/CH_3CN$ with 0.21 M $[(DMF)H]^+$ at scan rates of 1, 5, and 10 V/s. Conditions: 1 mm glassy carbon working electrode at 25 °C.

minimum scan rate threshold above which the observed behavior is that expected for a catalytic wave with no significant substrate depletion, as discussed in the Supporting Information.

Cyclic voltammetry studies were carried out on **5-OMe**, **5-Me**, **5-Br**, **5-Cl**, and **5-CF_3** as a function of acid concentration with sequential additions of $[(DMF)H]^+$ in CH_3CN at scan rates above those that showed i_{cat} independence (i.e., Figure 6, 5 and 10 V/s scan rates). Because of catalyst decomposition at high acid concentrations, addition was halted once an acid concentration greater than 0.40 M was attained, despite an apparent continuation of catalytic current enhancement. The length of these experiments was restricted to ca. 30 min, a period for which minimal (<5%) catalyst decomposition was observed under these acidic conditions, as determined by UV−vis spectroscopy for each complex (see the Supporting Information). The i_{cat} for each addition of acid was measured at the potential where the current first reaches its plateau (see the Supporting Information), and the ratio of i_{cat}/i_p can be used in eq 4 to calculate the rate constant k (υ = scan rate in V/s).[52,60−62] Assuming two electrons are passed for each H_2 molecule produced (n = 2), and the acid concentration does not change significantly during the course of the measurement (as indicated by a current plateau), the catalytic rate constant

dx.doi.org/10.1021/ja400181a | J. Am. Chem. Soc. 2013, 135, 6033−6046

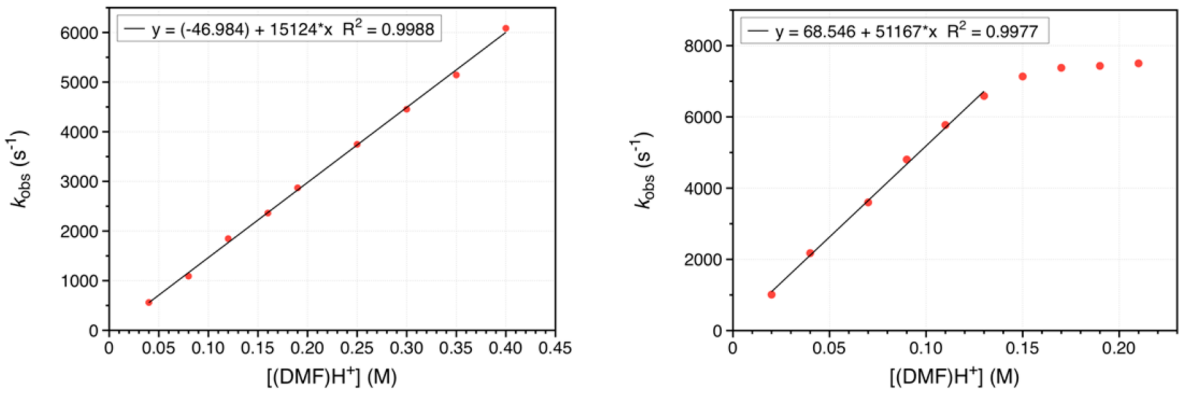

Figure 7. Plot of k_{obs} versus $[(DMF)H]^+$ for $[Ni(7P^{Ph}{}_2N^{C6H4X})_2]^{2+}$, (A) **5-Br** and (B) **5-OMe**, measured in 0.10 M $[Bu_4N][PF_6]/CH_3CN$ with increasing concentrations of $[(DMF)H]^+$. Conditions: 1 mm glassy carbon working electrode; 25 °C; scan rate 10 V/s.

Table 2. Electrocatalytic Data for Hydrogen Production

complex	overpotential[a] (mV)	$[(DMF)H]^+$ (M)	k_{obs} (s^{-1})	k (M^{-1} s^{-1})	$[(DMF)H]^+$, $[H_2O]$ (M)	k_{obs} (s^{-1})	k (M^{-1} s^{-1})
5-OMe	640	0.15	7500	51 000[b]	0.21, 0.52	22 000	
5-Me	630	0.39	27 000	69 000	0.41, 0.74	96 000	240 000
5-H[c]	625	0.43	33 000	77 000	0.42, 1.2	106 000	250 000
5-Br	580	0.40	6100	15 000	0.40, 0.74	17 000	42 000
5-Cl	580	0.43	4500	10 000	0.43, 1.0	15 000	34 000
5-CF_3	550	0.41	2400	6300	0.40, 0.81	4100	10 000

[a]As determined by the method of Evans for calculating overpotentials.[63] [b]Obtained for the linear region of the k_{obs} versus $[(DMF)H]^+$ before the acid-independent region. [c]As previously reported.[50]

($k_{obs} = k[H^+]^x$, eq 5), or turnover frequency, can be calculated using the simplified eq 6 (where T = 298 K). Using a constant acid concentration and measuring the i_{cat} as a function of catalyst concentration, the data also show a first-order dependence on catalyst concentration (see the Supporting Information).

$$\frac{i_{cat}}{i_p} = \frac{n}{0.4463}\sqrt{\frac{RT(k[H^+]^x)}{F\upsilon}} \quad (4)$$

$$k_{obs} = k[H^+]^x \quad (5)$$

$$k_{obs} = 1.94\ V^{-1}\cdot\upsilon\left(\frac{i_{cat}}{i_p}\right)^2 \quad (6)$$

Digital simulation of cyclic voltammograms of each Ni complex, in the absence of acid, allowed for the estimation of one-electron corrected i_p values, which differ from experimental i_p values featuring two electrons by a factor largely dependent upon peak overlap (i.e., ΔE_p, discussed further in the Supporting Information). While accounting for dilution, conservative i_p values were used to determine i_{cat}/i_p ratios to calculate k_{obs} for each acid addition. With the exception of **5-OMe**, plots of k_{obs} versus the acid concentration show first-order dependence (e.g., **5-Br**, Figure 7A) on acid concentration up to either 0.43 M $[(DMF)H]^+$ or until a 30 min experiment time, at which point decomposition of the catalyst becomes significant (<5%). For **5-OMe**, the observed rate constant becomes independent of acid concentration above 0.14 M $[(DMF)H]^+$ (Figure 7B). Higher concentrations of acid were not studied due to decomposition of each catalyst, resulting in unreliable measurements. From the plots of k_{obs} versus $[H^+]$, the second-order rate constants (first order in acid and first order in catalyst) were determined in the absence of added water and ranged from 6300 to 69 000 M^{-1} s^{-1} (Table 2). The catalytic production of H_2 was confirmed by quantitative gas chromatographic analysis of the H_2 produced during a controlled potential electrolysis experiment with **5-Me**. At a potential of −1.4 V and a $[(DMF)H]^+$ concentration of 0.2 M, a current efficiency of 99 ± 5% for H_2 production (11 turnovers) was observed.

On the basis of previous studies in which water was shown to significantly increase catalytic rates for $[Ni(P^R{}_2N^{R'}{}_2)_2](BF_4)_2$ complexes, aliquots of purified H_2O were added subsequent to the completion of acid additions, resulting in a further catalytic current enhancement (e.g., **5-Br**, Figure 4).[39−41] Water was added until the observed catalytic current enhancement ceased; the data are summarized in Table 2. The second-order rate constants k for **5-Me**, **5-Br**, **5-Cl**, and **5-CF_3** were found to range from 10 000 to 240 000 M^{-1} s^{-1} with the addition of water. For catalyst **5-OMe**, at acid concentrations above 0.15 M, the catalytic current and hence the catalytic rate become independent of the acid concentration, with a first-order rate constant (equivalent to the turnover frequency of the catalyst) of 22 000 s^{-1} in the presence of water (Figure 7B).

Detailed computational studies on **5-OMe**, **5-H**, and **5-CF_3** were carried out to gain further insights into the complex properties and the catalytic process and reported below.

DISCUSSION

Structural Effects on Catalyst Properties. X-ray diffraction studies of the new complexes **5-OMe**, **5-Me**, **5-Br**, **5-Cl**, and **5-CF_3** have shown that the smaller ring size of the heterocyclic ligand results in significant structural differences in

dx.doi.org/10.1021/ja400181a | J. Am. Chem. Soc. 2013, 135, 6033−6046

the complexes relative to the $[Ni(P^{R}_{2}N^{R'}_{2})_2]^{2+}$ series, and this in turn leads to substantial electronic differences that influence the catalytic activities. An important structural feature in each of the new complexes is the small P−Ni−P bite angle resulting from the $7P^{Ph}_{2}N^{C6H4X}$ ligand (79.7−80.1°). This small bite angle reduces the interligand steric interactions of the phenyl substituents of the phosphorus atoms of the two diphosphine ligands as compared to $[Ni(P^{Ph}_{2}N^{C6H4X}_{2})_2]^{2+}$ complexes, which have somewhat larger bite angles (82−84°).[39,40] As a result, all of the $[Ni(7P^{Ph}_{2}N^{C6H4X})_2]^{2+}$ cations exhibit planar structures with dihedral angles of 0.0° between the two planes defined by the phosphorus atoms of each diphosphine ligand and nickel. In previous studies of $[M(diphosphine)_2]^{2+}$ complexes (where M = Ni, Pd, and Pt), this dihedral angle has been shown to correlate with the potentials of M(II/I) couples.[64−66] The potentials of the Ni(II/I) couples shift to more negative values as the complexes become more planar, approaching the potentials of the M(I/0) couples. As a result, the potentials of the Ni(II/I) couples of the $[Ni(7P^{Ph}_{2}N^{C6H4X})_2]^{2+}$ complexes are more negative by 250−300 mV than those of the corresponding $[Ni(P^{Ph}_{2}N^{C6H4X}_{2})_2]^{2+}$ complexes, which have larger dihedral angles. The resulting redox waves associated with the Ni(II/I) and Ni(I/0) couples overlap for the $[Ni(7P^{Ph}_{2}N^{C6H4X})_2]^{2+}$ complexes due to the small difference in the Ni(II/I) and Ni(I/0) potentials ($\Delta E_{1/2}$). For example, simulations of cyclic voltammograms of **5-H** indicate a difference in redox potentials of 70 mV.[50] In contrast, these potentials differ by 190 mV for $[Ni(P^{Ph}_{2}N^{Ph}_{2})_2]^{2+}$.[39]

An extensive theoretical analysis of the structural, electrochemical, and acid/base properties of the **5-OMe**, **5-H**, and **5-CF_3** derivatives fully supports this interpretation. The calculated reduction potentials of the complexes are reported in Table 3. Overall, the experimentally measured (overlapping) potential for the Ni(II/I, I/0) processes and the calculated potentials for the Ni(II/I) and Ni(I/0) couples are in good agreement, with the Ni(I/0) couples occurring negative of the Ni(II/I) couples by 0.14 V or less. In particular, calculations semiquantitatively reproduce the shift toward more positive values for the Ni(II/I) couple from **5-OMe** to **5-CF_3**.

Table 3. Calculated Electrochemical Potentials (V) for $[Ni(7P^{Ph}_{2}N^{C6H4X})_2]^{2+}$ Complexes in CH_3CN

X	E(II/I)	E(I/0)
OMe	−1.07	−1.15
H	−1.04	−1.18
CF_3	−0.98	−1.07

The more negative potentials of the Ni(II/I) couples of the $[Ni(7P^{Ph}_{2}N^{C6H4X})_2]^{2+}$ derivatives compared to the $[Ni(P^{Ph}_{2}N^{C6H4X}_{2})_2]^{2+}$ analogues also correlate with the hydride donor abilities of their Ni(II) hydrides (eq 7). On the basis of previous correlations, the free energy for the heterolytic cleavage of the Ni−H bond in acetonitrile to form H^-, ΔG°_{H-}, is estimated to be 54.9 kcal/mol for $[HNi(7P^{Ph}_{2}N^{Ph})_2]^+$ (**5-H**), while that for $[HNi(P^{Ph}_{2}N^{Ph}_{2})_2]^+$ is 59.0 kcal/mol.[39,67,68] For the $[HNi(7P^{Ph}_{2}N^{C6H4X})_2]^+$ family, the ΔG°_{H-} values range from 54.5 for **5-OMe** to 56.0 kcal/mol for **5-CF_3**.

$$[HNi(7P^{Ph}_{2}N^{Ph})_2]^+ \underset{}{\overset{CH_3CN}{\rightleftharpoons}} [Ni(7P^{Ph}_{2}N^{Ph})_2]^{2+} + H^- \quad \Delta G^\circ_{H^-} = 54.9 \text{ kcal/mol} \qquad (7)$$

5-H

Mechanistic Studies. A likely ECEC mechanism for the formation of H_2 for the $[Ni(7P^{Ph}_{2}N^{C6H4X})_2]^{2+}$ complexes is proposed in Figure 8. The complexes are first electrochemically reduced (moving clockwise around Figure 8) to the Ni(I) species (ECEC), followed by protonation of a pendant amine (ECEC), and the second electron transfer (ECEC) to form the Ni(0) complex $[Ni(7P^{Ph}_{2}N^{C6H4X}H)(P^{Ph}_{2}N^{C6H4X})]^+$. This step is likely followed by an intramolecular proton transfer to form a Ni(II) hydride, $[HNi(7P^{Ph}_{2}N^{C6H4X})_2]^+$. Finally, the second protonation step (ECEC) occurs, followed by H−H bond formation, hydrogen elimination, and regeneration of the original catalyst.

Computational and experimental data support electron transfer followed by protonation of the Ni(I) species as the first steps in the catalytic process (Figure 8, steps 1−2). The calculated redox potentials for singly protonated Ni(II) complexes, $[Ni(7P^{Ph}_{2}N^{C6H4X}H)(P^{Ph}_{2}N^{C6H4X})]^{3+}$, resulting from protonation of **5-OMe**, **5-H**, and **5-CF_3**, are significantly more positive than those of the nonprotonated species (Table 4). For instance, the potential was calculated to be at −0.41 V for the Ni(II/I) couple of the singly endoprotonated complex derived from **5-H** (Table 4). When using $[(DMF)H]^+$ as the proton source (pK_a = 6.1 in CH_3CN),[57] the experimental data show catalysis occurring near the Ni(II/I)/(I/0) overlapping potentials (i.e., −1.1 V), supporting electron transfer as the first step in the mechanism. Additionally, computations indicate that singly protonated Ni(II) complexes (Table 4) are far more acidic than $[(DMF)H]^+$. Therefore, protonation at nitrogen prior to reduction of Ni(II) to Ni(I) is unlikely under catalytic conditions.

Table 4. Calculated Electrochemical Potentials (V) and pK_a Values in CH_3CN for Mono-protonated Ni(II) Complexes, $[Ni(7P^{Ph}_{2}N^{C6H4X}H)(7P^{Ph}_{2}N^{C6H4X})]^{3+}$

X	E(II/I)	E(I/0)	pK_a
OMe	−0.42	−0.49	−1.8
H	−0.41	−0.43	−3.0
CF_3	−0.30	−0.35	−5.3

We calculated the relative free energies and pK_a values of species that can form by reduction followed by protonation. The pK_a values for the lowest free energy isomers of the singly protonated Ni(I) isomers, $[Ni(7P^{Ph}_{2}N^{C6H4X}H)(P^{Ph}_{2}N^{C6H4X})]^{2+}$, are reported in Table 5. Protonation on the nitrogen atoms can occur endo to form **e(I)** (**e** indicating endo, **I** indicating the oxidation state of the metal, Figure 8, step 2_{endo}) or exo to form **x(I)** (**x** indicating exo protonation, Figure 8, step 2_{exo}), with respect to the metal center, resulting in the possibility of branching away from the main catalytic pathway. Calculations show that singly protonated Ni(I) exo isomers, **x(I)**, are systematically more acidic than the endo isomers **e(I)** by 3.7−4.5 pK_a units (Table 5). Consequently, **e(I)** isomers are more

Table 5. Calculated pK_a Values in CH_3CN for Endo and Exo Isomers of $[Ni(7P^{Ph}_{2}N^{C6H4X}H)(7P^{Ph}_{2}N^{C6H4X})]^{2+}$ and Endo Isomer of $[HNi(7P^{Ph}_{2}N^{C6H4X}H)(7P^{Ph}_{2}N^{C6H4X})]^{2+}$ (e/NiH)

X	e(I)	x(I)	e/NiH
OMe	7.7	4.0	10.3
H	5.9	1.4	8.9
CF_3	3.7	−0.2	6.8

dx.doi.org/10.1021/ja400181a | J. Am. Chem. Soc. 2013, 135, 6033−6046

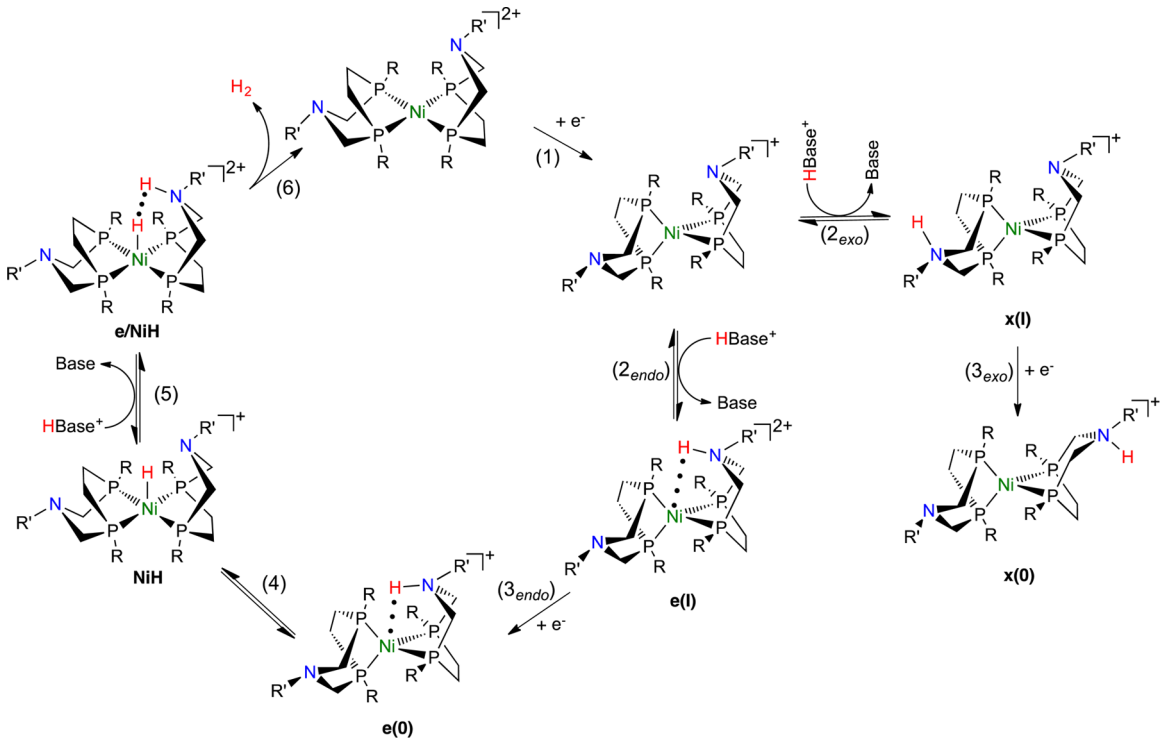

Figure 8. Proposed mechanism for catalytic H_2 formation.

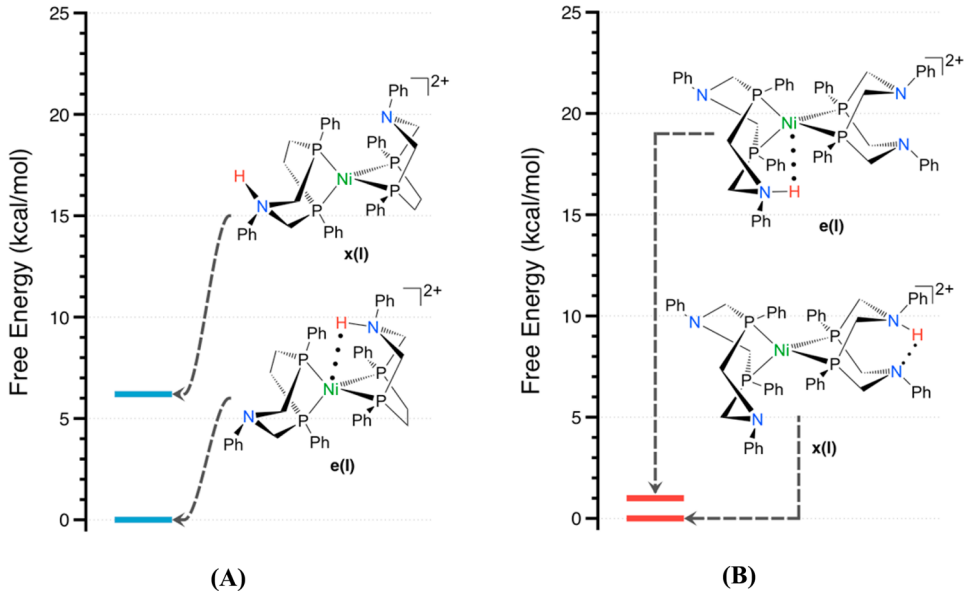

Figure 9. Ranking of the lowest free energy isomers of the singly protonated Ni(I) complexes of (A) $[Ni(7P^{Ph}{}_2N^{Ph}H)(7P^{Ph}{}_2N^{Ph})]^{2+}$ and (B) $[Ni(P^{Ph}{}_2N^{Ph}{}_2H)(P^{Ph}{}_2N^{Ph}{}_2)]^{2+}$.

stable than **x(I)** isomers (e.g., **5-H**, Figure 9A). This relative energy contrasts with the $[Ni(P^{Ph}{}_2N^{C6H4X}{}_2)_2]^{2+}$ catalysts, where the **x(I)** protonated species is stabilized by a NH···N hydrogen bond from the second pendant amine in the ligand,[69] resulting in stabilization of the **x(I)** species relative to the **e(I)** species (e.g., X = H, Figure 9B). As such, the relative pK_a values of the protonated pendant amines with respect to the pK_a of the proton source (i.e., the exogenous acid, protonated DMF in our studies) will play an important role in determining which protonation pathway is favored in both cases (Figure 8, step 2_{endo} or step 2_{exo}). In the $[Ni(7P^{Ph}{}_2N^{C6H4X})_2]^{2+}$ family, free energy calculations indicate protonation in the **e(I)** position will be favored in the case of **5-CF$_3$** and **5-H** (Figure 8, step 2_{endo}), as the pK_a of **x(I)** position lies 4−5 pK_a units more acidic than that of the proton source, $[(DMF)H]^+$. As the basicity of the pendant amine increases, however, exo protonation may start to play a role in the catalytic pathway. For example, in the case of **5-OMe**, the calculated pK_a values of both the **e(I)** and the **x(I)** complexes are only 1−2 pK_a units different from that of $[(DMF)H]^+$, so protonation to form the **x(I)** species likely becomes competitive (Figure 8, step 2_{exo}). The resulting effect may be an observed decrease in the catalytic rate of **5-OMe**, as

dx.doi.org/10.1021/ja400181a | J. Am. Chem. Soc. 2013, 135, 6033−6046

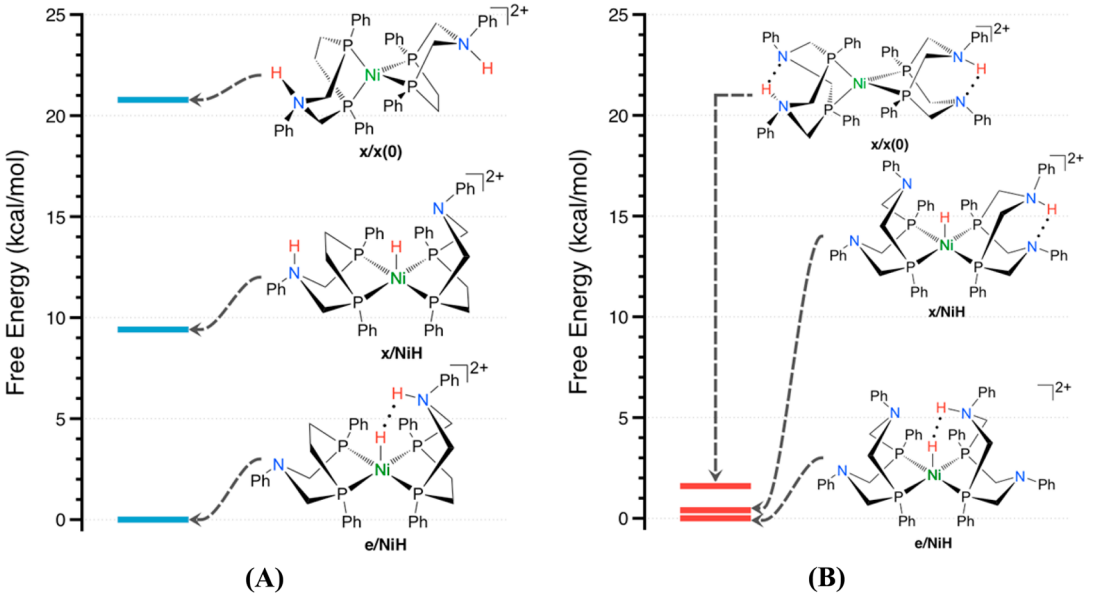

Figure 10. Ranking of the lowest free energy isomers of the doubly protonated complexes of (A) $[HNi(7P^{Ph}{}_2N^{C6H4X}H)(7P^{Ph}{}_2N^{C6H4X})]^{2+}$/$[Ni(7P^{Ph}{}_2N^{PhH})_2]^{2+}$ and (B) $[HNi(P^{Ph}{}_2N^{Ph}{}_2H)(P^{Ph}{}_2N^{Ph}{}_2)]^{2+}$/$[Ni(P^{Ph}{}_2N^{Ph}{}_2H)_2]^{2+}$.

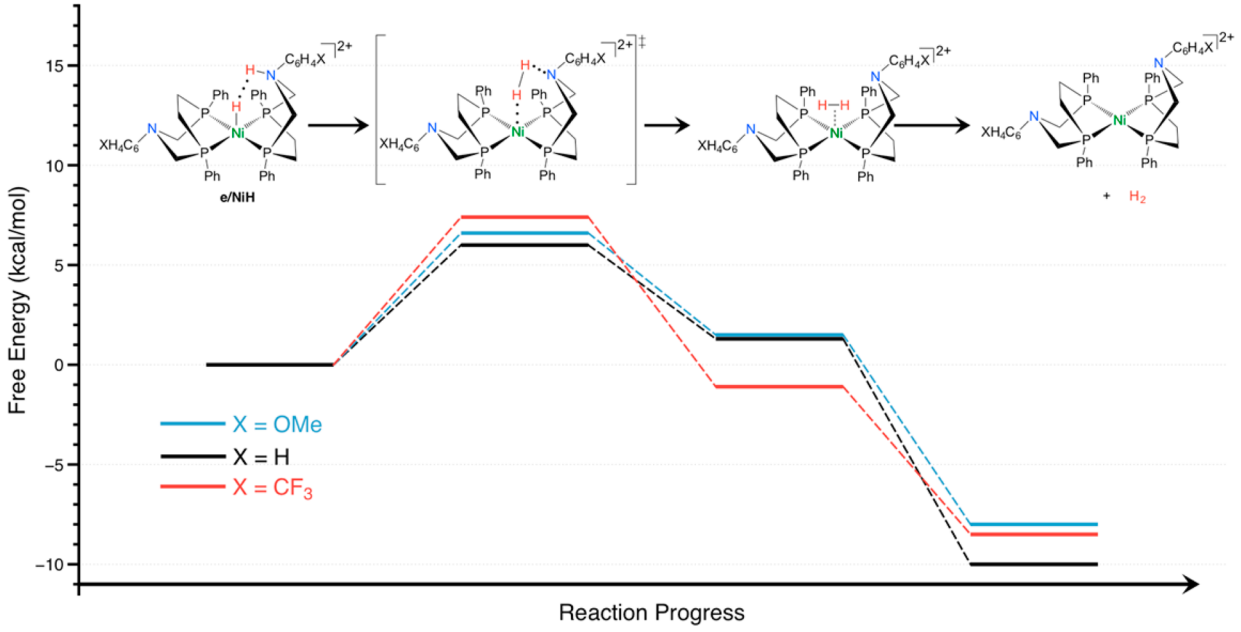

Figure 11. Lowest free energy H_2 elimination pathway for **5-OMe**, **5-H**, and **5-CF$_3$**.

protonation to generate **x(I)** becomes competitive and removes active catalyst from the cycle. As previously reported for the $[Ni(P^R{}_2N^{R'}{}_2)_2]^{2+}$ catalysts, exo protonation is thought to result in slower rates of catalytic hydrogen production, and that also appears to be the case for **5-OMe**.[48]

After protonation to form the Ni(I) species, $[Ni(7P^{Ph}{}_2N^{C6H4X}H)(7P^{Ph}{}_2N^{C6H4X})]^{2+}$, rapid reduction to Ni(0) likely occurs. As shown in Table 4, the calculated Ni(I/0) redox potential for the mono endoprotonated $[Ni(7P^{Ph}{}_2N^{C6H4X}H)(7P^{Ph}{}_2N^{C6H4X})]^{2+}$ species occurs between −0.49 and −0.35 V (Figure 8, step 3_{endo}) and is −0.71 V when protonated on exo site (Figure 8, step 3_{exo}), well positive of the Ni(II/I) redox couple for $[Ni(7P^{Ph}{}_2N^{C6H4X})_2]^{2+}$ complexes where catalysis occurs. As such, reduction and protonation to form the $[Ni(7P^{Ph}{}_2N^{C6H4X}H)(7P^{Ph}{}_2N^{C6H4X})]^{2+}$ species is expected to be rapidly followed by a second reduction to form $[Ni(7P^{Ph}{}_2N^{C6H4X}H)(7P^{Ph}{}_2N^{C6H4X})]^{+}$, which are Ni(0) complexes that are either endo **e(0)** or exo **x(0)** protonated at the pendant amine. Previous experimental and computational studies on $[Ni(P^R{}_2N^{R'}{}_2)_2]^{2+}$ have shown that endo protonated Ni(0) species rapidly isomerize to form Ni(II) hydride species.[47,70] Similarly, once reduction to form the N-protonated Ni(0) species, $[Ni(7P^{Ph}{}_2N^{C6H4X}H)(7P^{Ph}{}_2N^{C6H4X})]^{+}$, occurs, rapid intramolecular proton transfer likely follows (Figure 8, step 4), forming the Ni(II) hydride species $[HNi(7P^{Ph}{}_2N^{C6H4X})_2]^{+}$ (**NiH**). No such intramolecular isomerization is available for the **x(0)** species.

Protonation of the Ni(II) hydride species (**NiH**) can generate either an endo protonated hydride (**e/NiH**, Figure 8, step 5) or an exo protonated hydride (**x/NiH**) (see Figure

dx.doi.org/10.1021/ja400181a | J. Am. Chem. Soc. 2013, 135, 6033−6046

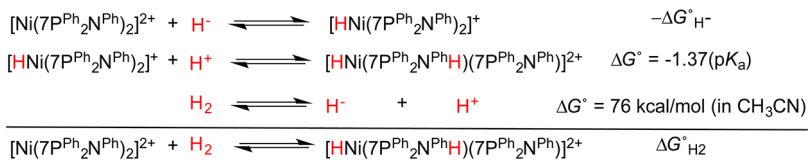

Figure 12. Themochemical cycle for the determination of the driving force for hydrogen addition, ΔG°_{H2}.

10).[38,47,48] Protonation of **x(0)** can occur in an endo position, relative to the nickel, yielding an **e/x(0)** species (which would undergo a rapid intramolecular isomerization to the exo protonated Ni(II) hydride, **x/NiH**, Figure 10) or exo, forming **x/x(0)** (Figure 10), a doubly protonated Ni(0) species. All of the doubly protonated species with exo positioned protons (**x/NiH** or **x/x(0)**), however, are calculated to be systematically higher in free energy than their endo counterpart (**e/NiH**). As shown in Figure 10, the energy differences between endo and exo species are even more pronounced for the second protonation than the first one (Figure 9). Given that the calculated pK_a values of the lowest energy intermediate (**e/NiH**) for **5-CF$_3$**, **5-H**, and **5-OMe** (Table 5) are greater than that of $[(DMF)H]^+$, whereas the calculated pK_a values of the **e(I)** intermediates are comparable to that of $[(DMF)H]^+$, it is postulated that the first protonation step, Ni(I) + $[(DMF)H]^+$ → **e(I)** + DMF, is the rate-determining step rather than the second protonation step, **NiH** + $[(DMF)H]^+$ → **e/NiH** + DMF.

In stark contrast to the $[Ni(7P^{Ph}{}_2N^{C6H4X})_2]^+$ family, protonation studies of the $[Ni(P^{R}{}_2N^{R'}{}_2)_2]^{2+}$ family of compounds, complemented by extensive theoretical modeling, indicate that the energy difference between endo and exo protonation is much smaller, and all isomers are populated under ambient conditions (Figure 9).[38,46−48] Indeed, the presence of the second pendant amine on each phosphine ligand allows the formation of exo hydrogen-bonded structures where the proton is "pinched" between two pendant amines, NH···N. In the case of $[Ni(P^{Ph}{}_2N^{Ph}{}_2)_2]^{2+}$, this hydrogen bond stabilizes the **x/x(0)** and **x/NiH** species, making their relative energies comparable (Figure 10).[38] The stability of the exo protonated species in the $[Ni(P^{Ph}{}_2N^{Ph}{}_2)_2]^{2+}$ family is thought to be a key factor in limiting their rate of catalysis, and one that the $[Ni(7P^{Ph}{}_2N^{C6H4X})_2]^+$ family has overcome.

Computational studies carried out on **5-CF$_3$**, **5-H**, and **5-OMe** show that, similarly to the $[Ni(P^{Ph}{}_2N^{Ph}{}_2)_2]^{2+}$ complex,[38] the evolution of hydrogen from the **e/NiH** species (Figure 8, step 6) proceeds in a heterolytic fashion through a transient dihydrogen Ni(II) complex, $[Ni(P^{Ph}{}_2N^{Ph})_2(H_2)]^{2+}$ (Figure 11).[38] The activation barriers calculated for this transition state range from 6.0 to 7.4 kcal/mol, far smaller than the barrier (>10 kcal/mol) inferred from the observed turnover frequency, further supporting the proposal that protonation of the Ni(I) species is the rate-determining step. The barrier for the subsequent H_2 elimination is believed to be low (smaller than those reported above), resulting in facile regeneration of the original Ni(II) catalysts.[38]

Interestingly, the overall free energy for H_2 elimination from the **e/NiH** intermediate ($-\Delta G^{\circ}_{H2}$) obtained from our quantum chemical calculations is more favorable for $[Ni(7P^{Ph}{}_2N^{Ph})_2]^+$ (**5-H**, $-\Delta G^{\circ}_{H2}$ = −10 kcal/mol) than for $[Ni(P^{Ph}{}_2N^{Ph}{}_2)_2]^{2+}$ ($-\Delta G^{\circ}_{H2}$ = −7.5 kcal/mol). As discussed previously,[71] ΔG°_{H2} is the result of a fine balance between the free energy for hydride transfer, ΔG°_{H-}, and the pK_a of the protonated pendant amine of **e/NiH**. This is evident from the thermodynamic cycle shown in Figure 12 (e.g., **5-H**). The more favorable $-\Delta G^{\circ}_{H2}$ for the $[Ni(7P^{Ph}{}_2N^{C6H4X})_2]^+$ complexes is a consequence of the greater hydride donor ability of $[HNi(7P^{Ph}{}_2N^{C6H4X})_2]^+$ discussed above, which dominates over the increased basicity of the pendant amine.

Of particular note from the kinetic studies of the $[Ni(7P^{Ph}{}_2N^{C6H4X})_2]^{2+}$ catalysts is the observation that they all show a first-order dependence on the concentration of acid. This indicates that, although two protonation steps must occur during the catalytic cycle, only one protonation step appears to be rate-determining for these catalysts. Evidence that the first protonation event may be rate-determining comes from analysis of the second-order rate constants derived from the observed rate constants for $[Ni(7P^{Ph}{}_2N^{C6H4X})_2]^{2+}$ catalysts (column 5 of Table 2) and the pK_a values of proposed intermediates. The calculated pK_a values of the **e/NiH** intermediates (Table 5) are greater than the pK_a of the $[(DMF)H]^+$ proton source (6.1), whereas the calculated pK_a values of the **e(I)** intermediates are comparable to or less than that of $[(DMF)H]^+$. As a result, it is reasonable to assume that the first protonation step, Ni(I) + $[(DMF)H]^+$ → **e(I)** + DMF (Figure 8, step 2), is the rate-determining step rather than the second protonation step, **NiH** + $[(DMF)H]^+$ → **e/NiH** + DMF (Figure 8, step 5).

A plot of the second-order rate conpstants observed for the $[Ni(7P^{Ph}{}_2N^{C6H4X})_2]^{2+}$ catalysts versus the pK_a values of the protonated amine of **e(I)**, ($[Ni(7P^{Ph}{}_2N^{C6H4X}H)(7P^{Ph}{}_2N^{C6H4X})]^{2+}$), shows the maximum rate constant occurring with the pendant amine that best matches the pK_a of the $[(DMF)H]^+$ proton source (Figure 13). The pK_a values of **e(I)** species derived from more acidic pendant amines than **5-H** (**5-CF$_3$**, **5-Cl** and **5-Br**) are below that of $[(DMF)H]^+$, resulting in slow (or incomplete) protonation. In complexes where the pendant amine substituents have a greater electron-donating

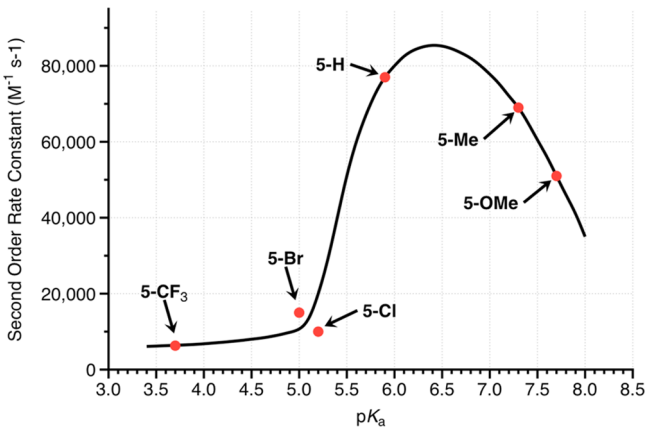

Figure 13. Graph of calculated pK_a values of the endo protonated, **e(I)** $[Ni(7P^{Ph}{}_2N^{C6H4X}H)(7P^{Ph}{}_2N^{C6H4X})]^{2+}$ complexes versus their second-order rate constants for hydrogen production. Black line between data points was added to illustrate the trend.

dx.doi.org/10.1021/ja400181a | J. Am. Chem. Soc. 2013, 135, 6033−6046

ability than the H atom in **5-H**, the pendant amine is basic enough to give rise to competitive exo protonation (Figure 8, step 2_{exo}), and the competitive formation of **x(I)** becomes likely. This competition is particularly pronounced in the case of the catalytic rate for **5-OMe**, which shows acid independence beyond 0.14 M $[(DMF)H]^+$, indicating the equilibrium between **e(I)** protonation/deprotonation plays a key role in limiting the overall catalytic process. Figure 13 illustrates the importance of pK_a matching between the pendant base and the exogenous base for relaying protons from the substrate to the metal via the pendant amines. Additionally, Figure 13 supports the proposed ECEC mechanism. An EECC mechanism would proceed through doubly protonated Ni(0) species that rapidly interconverts to the protonated Ni(II) hydride (Figure 8, **e/NiH**). Table 5 shows the pK_a values for the $[HNi(7P^{Ph}_2N^{C6H4X}H)(7P^{Ph}_2N^{C6H4X})]^{2+}$ (**e/NiH**) species are all greater than that of $[(DMF)H]^+$. Hence, if an EECC mechanism were occurring, the expected trend in Figure 13 would not be observed.

Effect of Water on Catalytic Rates. Addition of water (0.52−1.2 M) to reaction mixtures containing $[Ni(7P^{Ph}_2N^{C6H4X})_2]^{2+}$ complexes and $[(DMF)H]^+$ results in significant catalytic rate enhancements, as previously observed for the $[Ni(P^R_2N^{R'}_2)_2]^{2+}$ family of complexes.[39−41] Computational and experimental studies on the doubly protonated $[Ni(P^{Cy}_2N^{Bn}_2H)_2]^{2+}$ compounds suggest the rates of protonation and deprotonation of the pendant amines are hindered through steric interaction between phosphine substituents and the approaching substrate.[48] Indeed, the use of smaller substrates for proton delivery ($[(DMF)H]^+$ versus 2,5-dichloroanilinium) in the $[Ni(P^{Ph}_2N^{C6H4X}_2)_2]^{2+}$ family of catalysts resulted in higher rates. Additionally, in the family of $[Ni(P^R_2N^{Ph}_2)_2]^{2+}$ catalysts that contain bulky substituents at the phosphorus atoms, large increases in the rate of hydrogen production upon addition of water are attributed to more facile proton delivery through water acting as an intermolecular proton relay between the acid substrate and the pendant amine.[40] In the $[Ni(7P^{Ph}_2N^{C6H4X})_2]^{2+}$ complexes, water is proposed to function in a similar fashion, increasing the rate of protonation through the ease of access of small water molecules to the pendant amines, therefore shuttling protons from $[(DMF)H]^+$. Experimental and computation work to elucidate the exact role of water in these systems is ongoing in our laboratories.

CONCLUSIONS

The observation of high rates for H_2 formation with **5-OMe**, **5-Me**, **5-Br**, **5-Cl**, and **5-CF$_3$** clearly demonstrates that positioned proton relays in these catalysts play critical roles in all of the individual catalytic steps involving proton transfer and heterolytic formation of H_2. Comparisons of the $[Ni(7P^{Ph}_2N^{C6H4X})_2]^{2+}$ and $[Ni(P^{Ph}_2N^{C6H4X}_2)_2]^{2+}$ catalysts indicate that the increased planarity of the $[Ni(7P^{Ph}_2N^{C6H4X})_2]^{2+}$ complexes results in greater hydride donor abilities of $[HNi(7P^{Ph}_2N^{C6H4X})_2]^+$. The faster catalytic rates for H_2 production by $[Ni(7P^{Ph}_2N^{C6H4X})_2]^{2+}$ complexes are attributed to increased stability of endo versus exo protonation of the Ni(I) species due to the absence of the stabilizing NH···N "pinch" interaction that occurs in complexes with $P^{Ph}_2N^{C6H4X}_2$ ligands. The $[Ni(7P^{Ph}_2N^{C6H4X})_2]^+$ family of catalysts also clearly illustrates the importance of pK_a matching of the proton relay to the proton source in supporting rapid catalysis. Continuing studies currently underway in our laboratories are aimed at reducing the overpotential required to drive the electrocatalysis, while maintaining high turnover frequencies that are essential for producing an economically viable substitute for platinum.

EXPERIMENTAL SECTION

General Experimental Procedures. All manipulations with free phosphine ligands and metal reagents were carried out under N_2 using a standard vacuum line, Schlenk, and inert atmosphere glovebox techniques. Solvents were purified by passage through neutral alumina using an Innovative Technology, Inc., PureSolv solvent purification system. The 1,2-bis(phenylphosphino)ethane was purchased from Strem and used as received. Ferrocene was purchased from Aldrich and sublimed under vacuum before use. Tetrabutylammonium hexafluorophosphate, $[NBu_4][PF_6]$, was purchased from the Tokyo Chemical Industry (TCI) and recrystallized three times from absolute ethanol. H_2O was purified using a Millipore Milli-Q purifier and was sparged with nitrogen before use. The *meso/rac*-1,2-bis(hydroxymethylphenylphosphino)ethane,[51] $[(DMF)H]^+$,[55] and $[Ni(CH_3CN)_6](BF_4)_2$[72] were prepared according to literature procedures.

Instrumentation. NMR spectra were recorded on a Varian Inova spectrometer (500 MHz for ^1H) at 25 °C unless otherwise noted. All ^1H chemical shifts have been internally calibrated using the monoprotio impurity of the deuterated solvent. The $^{31}P\{^1H\}$ NMR spectra were referenced to external phosphoric acid at 0 ppm.

All experimental procedures were conducted at ambient temperature, 25 °C, under nitrogen using either standard Schlenk conditions or a Vacuum Atmospheres drybox. A standard three-electrode configuration was employed in conjunction with a CH Instruments potentiostat interfaced to a computer with CH Instruments 700 D software. All voltammetric scans were recorded using glassy carbon working electrode disks of 1 mm diameter (Cypress Systems EE040). The working electrode was treated between scans by a sequence of polishing with diamond paste (Buehler) of decreasing sizes (3 to 0.25 μm) interspersed by washings with purified H_2O. A glassy carbon rod (Structure Probe, Inc.) and platinum wire (Alfa-Aesar) were used as auxiliary electrodes and quasi-reference electrodes, respectively. All glassware for electrochemical experiments was oven-dried overnight and allowed to cool to room temperature before use. Ferrocene was used as an internal standard, and all potentials reported within this work are referenced to the ferrocenium/ferrocene couple at 0 V. Acids were measured and transferred to electrochemical solutions via an Eppendorf automatic micropipet.

meso/rac-7P$^{Ph}_2$N^{C6H4X} (**4-X**). To 1,2-bis(hydroxymethylphenylphosphino)ethane (1.5 g, 5.0 mmol) in 15 mL of CH_3CN at 75 °C was added the aniline reagent (5.0 mmol) as a 1.0 M CH_3CN solution, or by using a solid addition funnel, and the mixture was stirred at 75 °C for 12 h. Solvents were removed, leaving a white powder that was washed with diethyl ether (2 × 2 mL), dried under vacuum, and isolated as nearly a 50/50 mixture of the *meso*- and *rac*-isomers. **4-OMe**: Yield 1.61 g, 82%. $^{31}P\{^1H\}$ NMR (CD_3CN, ppm): −27.9 (s) and −29.4 (s). ^1H NMR (CD_3CN, ppm): 7.59−6.88 (multiple peaks, 14H, P−C_6H_5 and N−C_6H_4−OCH_3), 4.31−3.63 (multiple peaks, 4H, PCH_2N), 3.79 and 3.74 (s, 3H, N−C_6H_4−OCH_3), 2.52−2.23 (mult., 4H, PCH_2CH_2P). **4-Me**: Yield 1.23 g, 65%. $^{31}P\{^1H\}$ NMR (CD_2Cl_2, ppm): −26.9 (s) and −27.3 (s). ^1H NMR (CD_2Cl_2, ppm): 7.63−6.78 (multiple peaks, 14H, P−C_6H_5 and N−C_6H_4−CH_3), 4.28−3.43 (multiple peaks, 4H, PCH_2N), 4.69 and 4.64 (s, 3H, N−C_6H_4−CH_3) 2.62−2.31 (mult., 4H, PCH_2CH_2P). **4-Br**: Yield 1.88 g, 85%. $^{31}P\{^1H\}$ NMR (CD_3CN, ppm): −26.6 (s) and −27.0 (s). ^1H NMR (CD_3CN, ppm): 7.57−6.61 (multiple peaks, 14H, P−C_6H_5 and N−C_6H_4−Br), 4.31−3.61 (multiple peaks, 4H, PCH_2N), 2.49−2.18 (mult., 4H, PCH_2CH_2P). **4-Cl**: Yield 1.17 g, 59%. $^{31}P\{^1H\}$ NMR (CD_2Cl_2, ppm): −24.1 (s) and −24.4 (s). ^1H NMR (CD_2Cl_2, ppm): 7.48−7.09 (multiple peaks, 14H, P−C_6H_5, N−C_6H_4−Cl), 4.22−3.73 (multiple peaks, 4H, PCH_2N), 2.76−2.56 (mult., 4H, PCH_2CH_2P). **4-CF$_3$**: Yield 2.62 g, 74%. $^{31}P\{^1H\}$ NMR (CD_3CN, ppm): −25.5 (s) and −26.7 (s). ^1H NMR (CD_3CN, ppm): 7.46−6.64 (multiple peaks, 14H, P−C_6H_5 and N−C_6H_4−CF_3), 4.23−3.61 (multiple peaks, 14H, PCH_2N), 2.36−2.19 (mult., 4H, PCH_2CH_2P).

dx.doi.org/10.1021/ja400181a | J. Am. Chem. Soc. 2013, 135, 6033−6046

[Ni(7P$^{Ph}_2$N^{C6H4X})$_2$](BF$_4$)$_2$ (5-X). A mixture of the *meso*/*rac*-7P$^{Ph}_2$N^{C6H4X} ligand, **4-X**, (2.00 mmol) was combined with [Ni(CH$_3$CN)$_6$](BF$_4$)$_2$ (1.0 mmol) in 8 mL of CH$_3$CN forming a dark red solution that was stirred at room temperature for 1 h. Solvents were removed from the reaction solution, 2 mL of CH_2Cl_2 was added, followed by 5 mL of Et_2O upon which the product precipitated as orange crystalline needles. The product was isolated by filtration and washed with 2 × 2 mL of Et_2O. **5-OMe**: Yield 306 mg, 30%. Anal. Calcd for $C_{46}H_{50}B_2F_8N_2NiO_2P_4{\cdot}CH_3CN$: C, 54.38; H, 5.04; N, 3.96. Found: C, 54.34; H, 5.01; N, 3.74. $^{31}P\{^1H\}$ NMR (CD_2Cl_2, ppm): 44.6 (s). ^1H NMR (CD_2Cl_2, ppm): 7.14−6.83 (multiple peaks, 28H, C_6H_5 and $C_6H_4OCH_3$), 4.67−4.65 (mult., 4H, PCH_2N), 3.55−3.52 (mult., 4H, PCH_2N), 3.15−3.13 (mult., 4H, PCH_2CH_2P), 2.40−2.38 (mult., 4H, PCH_2CH_2P), 3.72 (s, 6H, $C_6H_4OCH_3$). **5-Me**: Yield 267 mg, 27%. $^{31}P\{^1H\}$ NMR (CD_2Cl_2, ppm): 44.3 (s). ^1H NMR (CD_2Cl_2, ppm): 7.83−6.94 (multiple peaks, 28H, C_6H_5 and $C_6H_4CH_3$), 4.71−4.68 (mult., 4H, PCH_2N), 3.79−3.76 (mult., 4H, PCH_2N), 3.06−3.03 (mult., 4H, PCH_2CH_2P), 2.34−2.32 (mult., 4H, PCH_2CH_2P), 2.25 (s, 6H, $C_6H_4CH_3$). **5-Br**: Yield 290 mg, 26%. Anal. Calcd for $C_{44}H_{44}B_2Br_2F_8N_2NiP_4{\cdot}CH_3CN$: C, 47.72; H, 4.09; N, 3.63. Found: C, 47.59; H, 3.98; N, 3.59. $^{31}P\{^1H\}$ NMR (CD_2Cl_2, ppm): 43.5 (s). ^1H NMR (CD_2Cl_2, ppm): 7.23−6.96 (multiple peaks, 28H, C_6H_5 and C_6H_4Br), 4.71−4.68 (mult., 4H, PCH_2N), 3.85−3.80 (mult., 4H, PCH_2N), 3.18−3.16 (mult., 4H, PCH_2CH_2P), 2.40−2.37 (mult., 4H, PCH_2CH_2P). **5-Cl**: Yield 360 mg, 35%. $^{31}P\{^1H\}$ NMR (CD_2Cl_2, ppm): 43.1 (s). ^1H NMR (CD_2Cl_2, ppm): 7.20−6.97 (multiple peaks, 28H, C_6H_5 and C_6H_4Cl), 4.75−4.71 (mult., 4H, PCH_2N), 3.81−3.78 (mult., 4H, PCH_2N), 3.20−3.17 (mult., 4H, PCH_2CH_2P), 2.41−2.39 (mult., 4H, PCH_2CH_2P). **5-CF$_3$** (X = CF$_3$): Yield 300 mg, 54%. Anal. Calcd for $C_{46}H_{44}B_2F_{14}N_2NiP_4$: C, 50.45; H, 4.05; N, 2.56. Found: C, 49.96; H, 4.37; N, 2.99. $^{31}P\{^1H\}$ NMR (CD_2Cl_2, ppm): 41.8 (s). ^1H NMR (CD_2Cl_2, ppm): 7.52−6.97 (multiple peaks, 28H, C_6H_5 and $C_6H_4CF_3$), 4.89−4.86 (mult., 4H, PCH_2N), 4.17−4.14 (mult., 4H, PCH_2N), 3.23−3.21 (mult., 4H, PCH_2CH_2P), 2.23−2.21 (mult., 4H, (PCH_2CH_2P). ^{19}F NMR (CD_2Cl_2, ppm, ref to C_6F_6): −58.57 and −144.64.

Computational Studies. Computational studies were carried out to gain further insights into the complex properties and the catalytic process. Molecular structures were optimized at the DFT level of theory with the hybrid B3P86[73,74] exchange and correlation functional. The Stuttgart-Dresden relativistic effective core potential and associated basis set[75] basis set were used for Ni, and Pople's 6-31G* was used for all nonmetal atoms. An additional polarization p function on protic and hydridic hydrogen atoms was included. Harmonic vibrational frequencies were calculated at the optimized geometries using the same level of theory to estimate the zero-point energy (ZPE) and the thermal contributions (298 K and 1 atm) to the gas-phase free energy. Free energies of solvation in acetonitrile (which include the change of thermodynamic conditions of P = 1 atm in the gas phase to 1 M solution) were then computed using a self-consistent reaction field (SCRF) model at the same level of theory as for the other steps. The conductor-like polarizable continuum model (CPCM)[76,77] was used with Bondi radii.[78] All geometries were optimized without any symmetry constraint and were verified by vibrational analyses at the same level of theory to ensure that they are minima on the potential energy surface. For some complexes, several conformations were considered, and the lowest energy conformer was chosen for the calculation of the thermodynamic properties. Acetonitrile was explicitly considered as fifth ligand for all of Ni(II) complexes. The pK_a values and redox potential were calculated according to the isodesmic scheme discussed by Chen et al.[79] The [Ni(P$^{Cy}_2$N$^{Bn}_2$)$_2$]$^{2+}$ system is used as reference for the pK_a calculations, and [Ni(P$^{Ph}_2$N$^{Ph}_2$)$_2$]$^{2+}$ for the redox potential. All of the calculations were carried out with Gaussian 09.[80]

The selection of hybrid B3P86 functional and basis set was shown to yield redox potentials, hydride donor strengths, and pK_a values with good accuracy for a set of complexes with various metals and ligands[79] and activation barriers for proton transfer and heterolytic H−H bond formation that compare favorably with CCSD(T) calculations level of theory.[43] However, the computational error due to the exchange and correlation functional and the continuum solvation model adopted can be as large as 2−3 kcal/mol.[38,43,81] Therefore, isomers separated by small free energy differences, such as the doubly protonated **e**/**NiH**, **x**/**NiH**, and **x**/**x** isomers of the Ni(P$^{Ph}_2$N$^{Ph}_2$)$_2$]$^{2+}$ complex (see Figure 10B), cannot be reliably ranked in free energy. Nevertheless, differences between the Ni(7P$^{Ph}_2$N^{Ph})$_2$]$^{2+}$ and [Ni(P$^{Ph}_2$N$^{Ph}_2$)$_2$]$^{2+}$ are meaningful, as they are larger than the expected error.

■ ASSOCIATED CONTENT

Supporting Information

Experimental details for **5-OMe**, **5-Me**, **5-Br**, **5-Cl**, and **5-CF$_3$** including electrochemical analysis, catalyst decomposition studies, catalytic scan-rate independence studies, catalytic production of hydrogen rates, reaction order with respect to catalyst, example calculation of k_{obs}, reaction order with respect to [(DMF)H]$^+$, determination of second-order rate constants, X-ray crystal data, and complete ref 80. This material is available free of charge via the Internet at http://pubs.acs.org.

■ AUTHOR INFORMATION

Corresponding Author

monte.helm@pnnl.gov

Notes

The authors declare no competing financial interest.

■ ACKNOWLEDGMENTS

We thank Dr. Daniel L. DuBois, Dr. Aaron M. Appel, and Dr. Shentan Chen for helpful discussions. This research was supported as part of the Center for Molecular Electrocatalysis, an Energy Frontier Research Center funded by the U.S. Department of Energy, Office of Science, Office of Basic Energy Sciences. Additional funding (Mary Lou Lindstrom and Colleen Thogerson) was provided by the U.S. Department of Energy Faculty and Student Team program. Computational resources were provided at W. R. Wiley Environmental Molecular Science Laboratory (EMSL), a national scientific user facility sponsored by the Department of Energy's Office of Biological and Environmental Research located at Pacific Northwest National Laboratory, and the National Energy Research Scientific Computing Center (NERSC) at Lawrence Berkeley National Laboratory. Pacific Northwest National Laboratory is operated by Battelle for the U.S. Department of Energy. We thank Dr. Jonathan Darmon for providing the cover artwork.

■ REFERENCES

(1) *Catalysis without Precious Metals*, 1st ed.; Bullock, R. M., Ed.; Wiley-VCH: New York, 2010.
(2) Frey, M. *ChemBioChem* **2002**, *3*, 153−160.
(3) Vincent, K. A.; Parkin, A.; Armstrong, F. A. *Chem. Rev.* **2007**, *107*, 4366−4413.
(4) Fontecilla-Camps, J. C.; Volbeda, A.; Cavazza, C.; Nicolet, Y. *Chem. Rev.* **2007**, *107*, 4273−4303.
(5) DuBois, D. L.; Bullock, R. M. *Eur. J. Inorg. Chem.* **2011**, 1017−1027.
(6) Artero, V.; Chavarot-Kerlidou, M.; Fontecave, M. *Angew. Chem., Int. Ed.* **2011**, *50*, 7238−7266.
(7) Sun, Y.; Bigi, J. P.; Piro, N. A.; Tang, M. L.; Long, J. R.; Chang, C. J. *J. Am. Chem. Soc.* **2011**, *133*, 9212−9215.
(8) Dempsey, J. L.; Brunschwig, B. S.; Winkler, J. R.; Gray, H. B. *Acc. Chem. Res.* **2009**, *42*, 1995−2004.
(9) Jacques, P.-A.; Artero, V.; Pecaut, J.; Fontecave, M. *Proc. Natl. Acad. Sci. U.S.A.* **2009**, *106*, 20627−20632.

(10) Jacobsen, G. M.; Yang, J. Y.; Twamley, B.; Wilson, A. D.; Bullock, R. M.; Rakowski DuBois, M.; DuBois, D. L. *Energy Environ. Sci.* **2008**, *1*, 167.
(11) Hu, X.; Brunschwig, B. S.; Peters, J. C. *J. Am. Chem. Soc.* **2007**, *129*, 8988−8998.
(12) Baffert, C.; Artero, V.; Fontecave, M. *Inorg. Chem.* **2007**, *46*, 1817−1824.
(13) Razavet, M.; Artero, V.; Fontecave, M. *Inorg. Chem.* **2005**, *44*, 4786−4795.
(14) Wiedner, E. S.; Yang, J. Y.; Dougherty, W. G.; Kassel, W. S.; Bullock, R. M.; Rakowski DuBois, M.; DuBois, D. L. *Organometallics* **2010**, *29*, 5390−5401.
(15) Rose, M. J.; Gray, H. B.; Winkler, J. R. *J. Am. Chem. Soc.* **2012**, *134*, 8310−8315.
(16) Camara, J. M.; Rauchfuss, T. B. *Nat. Chem.* **2012**, *4*, 26−30.
(17) Singleton, M. L.; Crouthers, D. J.; Duttweiler, R. P.; Reibenspies, J. H.; Darensbourg, M. Y. *Inorg. Chem.* **2011**, *50*, 5015−5026.
(18) Camara, J. M.; Rauchfuss, T. B. *J. Am. Chem. Soc.* **2011**, *133*, 8098−8101.
(19) Gloaguen, F.; Rauchfuss, T. B. *Chem. Soc. Rev.* **2009**, *38*, 100−108.
(20) Barton, B. E.; Olsen, M. T.; Rauchfuss, T. B. *J. Am. Chem. Soc.* **2008**, *130*, 16834−16835.
(21) Justice, A. K.; De Gioia, L.; Nilges, M. J.; Rauchfuss, T. B.; Wilson, S. R.; Zampella, G. *Inorg. Chem.* **2008**, *47*, 7405−7414.
(22) Barton, B. E.; Rauchfuss, T. B. *Inorg. Chem.* **2008**, *47*, 2261−2263.
(23) Tard, C.; Liu, X.; Ibrahim, S. K.; Bruschi, M.; De Gioia, L.; Davies, S. C.; Yang, X.; Wang, L.-S.; Sawers, G.; Pickett, C. J. *Nature* **2005**, *433*, 610−613.
(24) Mejia-Rodriguez, R.; Chong, D.; Reibenspies, J. H.; Soriaga, M. P.; Darensbourg, M. Y. *J. Am. Chem. Soc.* **2004**, *126*, 12004−12014.
(25) Chong, D.; Georgakaki, I. P.; Mejia-Rodriguez, R.; Sanabria-Chinchilla, J.; Soriaga, M. P.; Darensbourg, M. Y. *Dalton Trans.* **2003**, *0*, 4158−4163.
(26) Gloaguen, F.; Lawrence, J. D.; Rauchfuss, T. B.; Bénard, M.; Rohmer, M.-M. *Inorg. Chem.* **2002**, *41*, 6573−6582.
(27) Gloaguen, F.; Lawrence, J. D.; Rauchfuss, T. B. *J. Am. Chem. Soc.* **2001**, *123*, 9476−9477.
(28) Darensbourg, M. Y.; Lyon, E. J.; Smee, J. J. *Coord. Chem. Rev.* **2000**, *206*, 533−561.
(29) Karunadasa, H. I.; Montalvo, E.; Sun, Y.; Majda, M.; Long, J. R.; Chang, C. J. *Science* **2012**, *335*, 698−702.
(30) Karunadasa, H. I.; Chang, C. J.; Long, J. R. *Nature* **2010**, *464*, 1329−1333.
(31) Appel, A. M.; DuBois, D. L.; Rakowski DuBois, M. *J. Am. Chem. Soc.* **2005**, *127*, 12717−12726.
(32) Thoi, V. S.; Sun, Y.; Long, J. R.; Chang, C. J. *Chem. Soc. Rev.* **2013**, DOI: 10.1039/C2CS35272A.
(33) Wang, M.; Chen, L.; Sun, L. *Energy Environ. Sci.* **2012**, *5*, 6763−6778.
(34) Rakowski DuBois, M.; DuBois, D. L. *Acc. Chem. Res.* **2009**, *42*, 1974−1982.
(35) Rakowski DuBois, M.; DuBois, D. L. *Chem. Soc. Rev.* **2009**, *38*, 62−72.
(36) Liu, T.; Chen, S.; O'Hagan, M. J.; Rakowski DuBois, M.; Bullock, R. M.; DuBois, D. L. *J. Am. Chem. Soc.* **2012**, *134*, 6257−6272.
(37) Welch, K. D.; Dougherty, W. G.; Kassel, W. S.; DuBois, D. L.; Bullock, R. M. *Organometallics* **2010**, *29*, 4532−4540.
(38) Raugei, S.; Chen, S.; Ho, M.-H.; Ginovska-Pangovska, B.; Rousseau, R. J.; Dupuis, M.; DuBois, D. L.; Bullock, R. M. *Chem.-Eur. J.* **2012**, *18*, 6493−6506.
(39) Kilgore, U. J.; Roberts, J. A. S.; Pool, D. H.; Appel, A. M.; Stewart, M. P.; Rakowski DuBois, M.; Dougherty, W. G.; Kassel, W. S.; Bullock, R. M.; DuBois, D. L. *J. Am. Chem. Soc.* **2011**, *133*, 5861−5872.
(40) Kilgore, U. J.; Stewart, M. P.; Helm, M. L.; Dougherty, W. G.; Kassel, W. S.; Rakowski DuBois, M.; DuBois, D. L.; Bullock, R. M. *Inorg. Chem.* **2011**, *50*, 10908−10918.
(41) Wiese, S.; Kilgore, U. J.; DuBois, D. L.; Bullock, R. M. *ACS Catal.* **2012**, *2*, 720−727.
(42) Smith, S. E.; Yang, J. Y.; DuBois, D. L.; Bullock, R. M. *Angew. Chem., Int. Ed.* **2012**, *51*, 3152−3155.
(43) Chen, S.; Raugei, S.; Rousseau, R. J.; Dupuis, M.; Bullock, R. M. *J. Phys. Chem. A* **2010**, *114*, 12716−12724.
(44) Dupuis, M.; Chen, S.; Raugei, S.; DuBois, D. L.; Bullock, R. M. *J. Phys. Chem. A* **2011**, *115*, 4861−4865.
(45) Yang, J. Y.; Bullock, R. M.; Shaw, W. J.; Twamley, B.; Fraze, K.; Rakowski DuBois, M.; DuBois, D. L. *J. Am. Chem. Soc.* **2009**, *131*, 5935−5945.
(46) Appel, A. M.; Pool, D. H.; O'Hagan, M. J.; Shaw, W. J.; Yang, J. Y.; Rakowski DuBois, M.; DuBois, D. L.; Bullock, R. M. *ACS Catal.* **2011**, *1*, 777−785.
(47) O'Hagan, M. J.; Shaw, W. J.; Raugei, S.; Chen, S.; Yang, J. Y.; Kilgore, U. J.; DuBois, D. L.; Bullock, R. M. *J. Am. Chem. Soc.* **2011**, *133*, 14301−14312.
(48) O'Hagan, M. J.; Ho, M.-H.; Yang, J. Y.; Appel, A. M.; Rakowski DuBois, M.; Raugei, S.; Shaw, W. J.; DuBois, D. L.; Bullock, R. M. *J. Am. Chem. Soc.* **2012**, *134*, 19409−19424.
(49) Wilson, A. D.; Newell, R. H.; McNevin, M. J.; Muckerman, J. T.; Rakowski DuBois, M.; DuBois, D. L. *J. Am. Chem. Soc.* **2006**, *128*, 358−366.
(50) Helm, M. L.; Stewart, M. P.; Bullock, R. M.; Rakowski DuBois, M.; DuBois, D. L. *Science* **2011**, *333*, 863−866.
(51) Karasik, A. A.; Balueva, A. S.; Moussina, E. I.; Naumov, R. N.; Dobrynin, A. B.; Krivolapov, D. B.; Litvinov, I. A.; Sinyashin, O. G. *Heteroat. Chem.* **2008**, *19*, 125−132.
(52) Bard, A. J.; Faulkner, L. R. *Electrochemical Methods: Fundamentals and Applications*, 2nd ed.; Wiley: New York, 2000.
(53) Lever, A. B. P. *Inorg. Chem.* **1990**, *29*, 1271−1285.
(54) Lu, S.; Strelets, V. V.; Ryan, M. F.; Pietro, W. J.; Lever, A. B. P. *Inorg. Chem.* **1996**, *35*, 1013−1023.
(55) Favier, I.; Duñach, E. *Tetrahedron Lett.* **2004**, *45*, 3393−3395.
(56) Kolthoff, I. M.; Chantooni, M. K.; Bhowmik, S. *Anal. Chem.* **1967**, *39*, 1627−1633.
(57) Izutsu, K. *Acid-Base Dissociation Constants in Dipolar Aprotic Solvents*; Blackwell Scientific Publications: Cambridge, MA, 1990.
(58) Delahay, P.; Stiehl, G. L. *J. Am. Chem. Soc.* **1952**, *74*, 3500−3505.
(59) Nicholson, R. S.; Shain, I. *Anal. Chem.* **1964**, *36*, 706−723.
(60) Savéant, J. M.; Vianello, E. *Electrochim. Acta* **1965**, *10*, 905−920.
(61) Savéant, J. M.; Vianello, E. *Electrochim. Acta* **1967**, *12*, 629−646.
(62) Savéant, J. M. *Acc. Chem. Res.* **1980**, *13*, 323−329.
(63) Felton, G. A. N.; Glass, R. S.; Lichtenberger, D. L.; Evans, D. H. *Inorg. Chem.* **2006**, *45*, 9181−9184.
(64) Raebiger, J. W.; Miedaner, A.; Curtis, C. J.; Miller, S. M.; Anderson, O. P.; DuBois, D. L. *J. Am. Chem. Soc.* **2004**, *126*, 5502−5514.
(65) Curtis, C. J.; Miedaner, A.; Raebiger, J. W.; DuBois, D. L. *Organometallics* **2004**, *23*, 511−516.
(66) Berning, D. E.; Noll, B. C.; DuBois, D. L. *J. Am. Chem. Soc.* **1999**, *121*, 11432−11447.
(67) Wilson, A. D.; Fraze, K.; Twamley, B.; Miller, S. M.; DuBois, D. L.; Rakowski DuBois, M. *J. Am. Chem. Soc.* **2008**, *130*, 1061−1068.
(68) Berning, D. E.; Miedaner, A.; Curtis, C. J.; Noll, B. C.; Rakowski DuBois, M.; DuBois, D. L. *Organometallics* **2001**, *20*, 1832−1839.
(69) Wiedner, E. S.; Yang, J. Y.; Chen, S.; Raugei, S.; Dougherty, W. G.; Kassel, W. S.; Helm, M. L.; Bullock, R. M.; Rakowski DuBois, M.; DuBois, D. L. *Organometallics* **2012**, *31*, 144−156.
(70) Horvath, S.; Fernandez, L. E.; Soudackov, A. V.; Hammes-Schiffer, S. *Proc. Natl. Acad. Sci. U.S.A.* **2012**, *109*, 15663−15668.
(71) Fraze, K.; Wilson, A. D.; Appel, A. M.; Rakowski DuBois, M.; DuBois, D. L. *Organometallics* **2007**, *26*, 3918−3924.
(72) Hathaway, B. J.; Holah, D. G.; Underhill, A. E. *J. Chem. Soc.* **1962**, 2444−2448.
(73) Perdew, J. P. *Phys. Rev. B* **1986**, *33*, 8822−8824.
(74) Becke, A. D. *J. Chem. Phys.* **1993**, *98*, 5648.

(75) Andrae, D.; Häußermann, U.; Dolg, M.; Stoll, H.; Preuß, H. *Theor. Chim. Acta* **1990**, *77*, 123−141.
(76) Cossi, M.; Rega, N.; Scalmani, G.; Barone, V. *J. Comput. Chem.* **2003**, *24*, 669−681.
(77) Barone, V.; Cossi, M. *J. Phys. Chem. A* **1998**, *102*, 1995−2001.
(78) Bondi, A. *J. Phys. Chem.* **1964**, *68*, 441−451.
(79) Chen, S.; Rousseau, R. J.; Raugei, S.; Dupuis, M.; DuBois, D. L.; Bullock, R. M. *Organometallics* **2011**, *30*, 6108−6118.
(80) Frisch, M. J.; et al. *Gaussian 09*, revision B01; Gaussian, Inc.: Wallingford, CT, 2009.
(81) Liakos, D. G.; Hansen, A.; Neese, F. *J. Chem. Theory Comput.* **2011**, *7*, 76−87.